RESEARCH

Skull of a new periptychid mammal from the lower Paleocene Denver Formation of Colorado (Corral Bluffs, El Paso County)

Lucas N. Weaver[1,6] · Jordan W. Crowell[2,3] · Stephen G. B. Chester[2,3,4] · Tyler R. Lyson[5]

Abstract

The Periptychidae, an extinct group of archaic ungulates ('condylarths'), were the most speciose eutherian mammals in the earliest Paleocene of North America, epitomizing mammalian ascendency after the Cretaceous–Paleogene (K–Pg) mass extinction. Although periptychids are mostly known from fragmentary gnathic remains, the Corral Bluffs area within the Denver Basin, Colorado, has yielded numerous exceptionally well-preserved mammalian fossils, including periptychids, from the earliest Paleocene. Here we describe a partial cranium and articulated dentaries plus an additional unassociated dentary fragment of a small-bodied (~273–455 g) periptychid from ca. 610 thousand years after the K–Pg mass extinction (Puercan 2 North American Land Mammal 'age') at Corral Bluffs. Based on these new fossils we erect *Militocodon lydae* gen. et sp. nov. The dentition of *M. lydae* exhibits synapomorphies that diagnose the Conacodontinae, but it is plesiomorphic relative to *Oxyacodon*, resembling putatively basal periptychids like *Mimatuta* and *Maiorana* in several dental traits. As such, we interpret *M. lydae* as a basal conacodontine. Its skull anatomy does not reveal clear periptychid synapomorphies and instead resembles that of arctocyonids and other primitive eutherians. *M. lydae* falls along a dental morphocline from basal periptychids to derived conacodontines, which we hypothesize reflects a progressive, novel modification of the hypocone to enhance orthal shearing and crushing rather than grinding mastication. The discovery and thorough descriptions and comparisons of the partial *M. lydae* skull represent an important step toward unraveling the complex evolutionary history of periptychid mammals.

Lucas N. Weaver and Jordan W. Crowell contributed equally to this work.

✉ Lucas N. Weaver
lukeweav@umich.edu

✉ Jordan W. Crowell
jcrowell@gradcenter.cuny.edu

1 Department of Earth Sciences, Kent State University, Kent, OH 44242, USA

2 PhD Program in Anthropology, The Graduate Center, City University of New York, New York, NY 10016, USA

3 New York Consortium in Evolutionary Primatology, New York, NY 10024, USA

4 Department of Anthropology, Brooklyn College, City University of New York, Brooklyn, NY 11210, USA

5 Department of Earth Sciences, Denver Museum of Nature & Science, Denver, CO 80205, USA

6 Museum of Paleontology, Department of Earth and Environmental Sciences, University of Michigan, Ann Arbor, MI 48109, USA

Introduction

Archaic ungulates (i.e., 'condylarths') are a taxonomically contentious group that likely gave rise to extant hooved mammals (Archibald 1998) and whose initial diversification epitomizes the rise of eutherians in the early aftermath of the Cretaceous–Paleogene (K–Pg) mass extinction in North America (e.g., Simpson 1937a; Archibald 1982; Eberle and Lillegraven 1998; Alroy 1999; Clemens 2002; Wilson 2014; Lyson et al. 2019). Archaic ungulates first appear in the lowermost Paleocene (Danian), defining the onset of the Puercan North American Land Mammal 'age' (NALMA; Lofgren et al. 2004; but see Johnston and Fox 1984, Archibald et al. 2011, and Kelly 2014 for putative records of latest Cretaceous archaic ungulates), and within less than 300 thousand years (ka) after the K–Pg boundary (e.g., Wilson 2014; Smith et al. 2018; Wilson Mantilla et al. 2021; Claytor et al. 2022) they became the most species-rich group of eutherian mammals (Fig. 1).
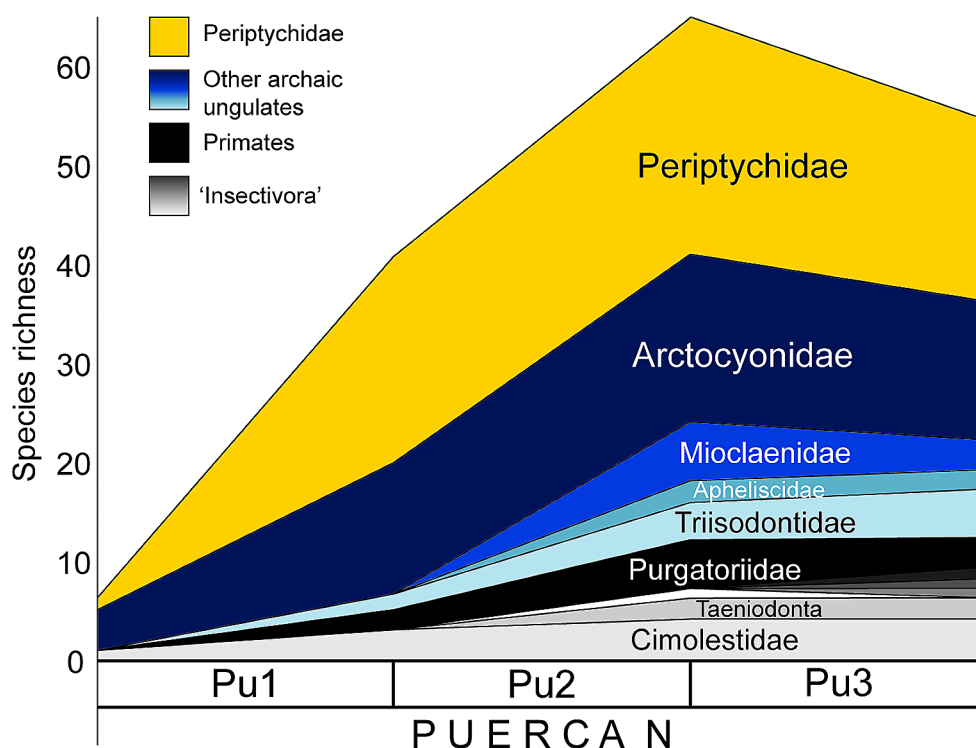
Fig. 1 Raw species richness of eutherian mammal families from the Puercan North American Land Mammal 'age' (NALMA), subdivided into Puercan (Pu) 1, 2, and 3 subintervals, capturing roughly the first one million years of the Paleocene. Note the high species richness of periptychids relative to all other eutherian families. Species richness data were compiled from Lofgren et al. (2004), Silviria (2019), Atteberry and Eberle (2021), and Wilson Mantilla et al. (2021). Note that the white portion between Purgatoriidae and Taeniodonta represents the putative carnivoran *Ravenictis krausei*, Arctocyonidae includes taxa (e.g., *Carcinodon*) that were previously considered oxyclaenids (see Williamson and Carr 2007), and taxa included in the Mioclaenidae and Apheliscidae have been variously referred to the Hyopsodontidae (see Zack et al. 2005 and Williamson and Weil 2011). Duration of the Puercan NALMA is incompletely resolved and not taxonomically or temporally homogeneous across different basins, but see Sprain et al. (2018), Lyson et al. (2019), and Flynn et al. (2020) for the most recent temporal constraints in the Williston, Denver, and San Juan basins, respectively

The rapid diversification of early archaic ungulates was driven in large part by the Periptychidae, which accounted for nearly half of archaic ungulate species richness in the Puercan (Fig. 1). Periptychids are characterized by bulbous, bunodont cheek teeth with enlarged posterior premolars, lingually sloping molar protocones and hypocones, and closely appressed molar cusps (Matthew 1937; Simpson 1937b; Archibald 1998). The phylogenetic position of periptychids among Placentalia is uncertain, but recent analyses have suggested that they are nested among Laurasiatheria (e.g., Zack 2009). Given their dental apomorphies, the monophyly and generic membership of the Periptychidae has remained reasonably stable relative to other, more dentally plesiomorphic or conserved archaic ungulate groups such as the Arctocyonidae and Hyopsodontidae that are less well-defined. Nonetheless, the generic and specific constituents of the periptychid subgroups—Periptychinae, Anisonchinae, Conacodontinae—have fluctuated substantially (e.g., Archibald et al. 1983a, b), with some likely being paraphyletic (e.g., Anisonchinae; Archibald 1993, 1998; Shelley 2018). Further, recent phylogenetic hypotheses propose that

Mimatuta and *Maiorana*, two genera traditionally considered basal periptychids (Van Valen 1978; Archibald 1998), do not belong in the Periptychidae (Shelley 2018; Atteberry and Eberle 2021), raising questions about periptychid character polarity and evolutionary trends.

Like for most early Paleocene mammals, the uncertainties surrounding the systematics of the Periptychidae are due in part to their fossil record, comprised mostly of isolated teeth and jaw fragments, with associated upper and lower dentitions and more complete skeletal fossils being rare. Indeed, relatively complete periptychid cranial remains are only known from the periptychines *Periptychus*, *Ectoconus*, and *Carsioptychus* (e.g., Matthew 1937; Shelley et al. 2018; Lyson et al. 2019), the anisonchine *Haploconus* (Matthew 1937), and the putative basal periptychid *Maiorana* (reported but undescribed; Van Valen 1978). Most of these taxa are morphologically derived, large-bodied, and geologically young members of the clade (e.g., Matthew 1937; Shelley 2018) and have only been cursorily described. The cranial morphology of the Conacodontinae remains unknown. As such, what cranial apomorphies characterize

the Periptychidae and when in geologic time those cranial morphologies arose remains unclear.

Here we describe the partial skull and additional dentary fragment of a small-bodied periptychid (273–455 g; see 'Materials and methods' below) from the Puercan 2 (Pu2) of the Corral Bluffs area in the Denver Basin, Colorado (Fig. 2). To date, Corral Bluffs has yielded hundreds of exceptionally preserved fossil vertebrates, including nearly 100 mammalian fossils consisting of skulls, jaws, and postcrania (Lyson et al. 2019; Krause et al. 2021). Based on these new fossils we erect *Militocodon lydae* gen. et sp. nov., which we interpret as a basal conacodontine. The craniodental morphology of *M. lydae* sheds new light on the early evolutionary history of the Periptychidae and highlights the importance of the Corral Bluffs mammalian fossil record for understanding the rise of eutherian mammals in the aftermath of the K–Pg mass extinction.

Institutional abbreviations: AMNH, American Museum of Natural History, New York, New York, USA. **DMNH**, Denver Museum of Nature & Science, Denver, Colorado, USA. **MNHN.F**, Fossil cranium collections at the Muséum national d'Histoire naturelle, Paris, France. **NMMNH P**, Paleontological collections at the New Mexico Museum of Natural History & Science, Albuquerque, New Mexico, USA. **UCM**, University of Colorado Museum of Natural History, Boulder, Colorado, USA. **UCMP**, University of California Museum of Paleontology, Berkeley, California, USA. **YPM-PU**, Princeton University Collection at the Yale Peabody Museum, New Haven, Connecticut, USA.

Geologic setting

Corral Bluffs is located east of Colorado Springs, Colorado, USA, and is situated within the Denver Basin (Fig. 2c). The south-facing arc of exposures that make up Corral Bluffs are part of the D1 sequence of the Denver Formation, which spans the uppermost Cretaceous through lower Paleocene (Fig. 2d; Raynolds 2002). Corral Bluffs is located near the Rocky Mountain Front Range and exposures of the D1 sequence at Corral Bluffs are much coarser grained than those in the eastern, mountain-distal portions of the Denver Basin which preserve comparably aged sediments (Barclay et al. 2003). Corral Bluffs outcrops are characterized by stratigraphically thick (~10 m), laterally persistent (> 100 m), medium-to-coarse-grained trough cross-bedded fluvial-channel sandstones interbedded with siltstones or silty-to-sandy claystones (Raynolds 1997, 2002; Lyson et al. 2019).

Corral Bluffs chronostratigraphy is anchored by a combination of mammalian biostratigraphy (Brown 1943; Eberle 2003; Lyson et al. 2019), palynostratigraphy (Lyson et al. 2019), magnetostratigraphy (Hicks et al. 2003; Fuentes et al. 2019), the Geomagnetic Polarity Time Scale (GPTS; Gradstein et al. 2012), and radiometric dating (Fuentes et al. 2019; Lyson et al. 2019) (Fig. 2d). The K–Pg boundary has also been identified in the eastern portions of the Denver Basin via an iridium anomaly, shocked minerals, and palynostratigraphy (Barclay et al. 2003; Nichols and Fleming 2002) and at Corral Bluffs via palynostratigraphy (Fuentes
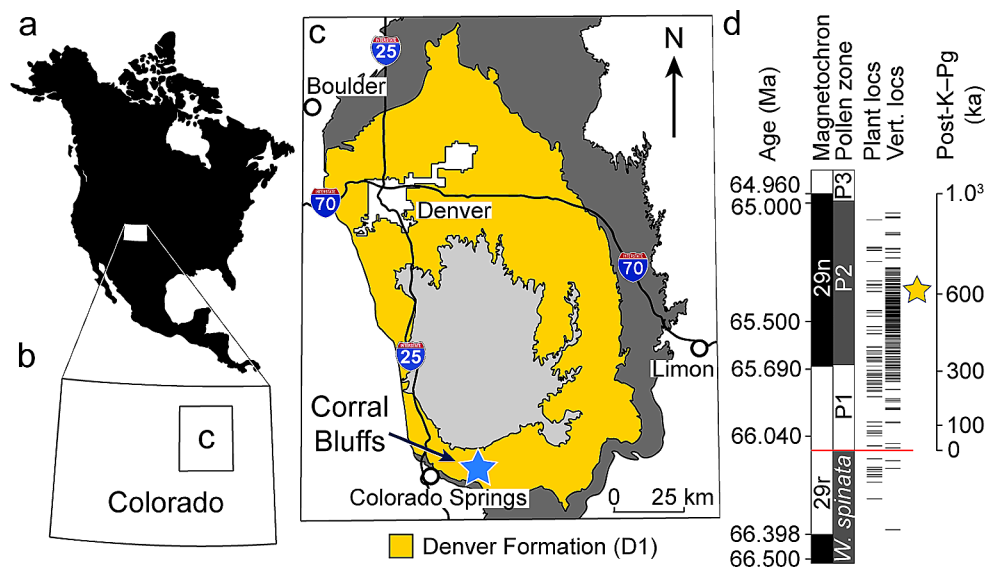

Fig. 2 Corral Bluffs study area and chronostratigraphic location of the fossils described here. **a**. North America; **b**. Colorado; **c**. Denver Basin and coarse geologic map of exposures of the D1 sequence of the Denver Formation, which spans the uppermost Cretaceous and lowermost Paleocene. Corral Bluffs is represented by the blue star just east of Colorado Springs. **d**. Chronostratigraphic framework and distribution of plant and vertebrate fossil localities at Corral Bluffs (see text and references therein). DMNH EPV.136181 and 103390 (yellow star) were found 97–101 m above the K–Pg boundary (denoted by red line), corresponding to an approximate age of 610 ka after the K–Pg mass extinction. Abbreviations: **ka**, thousands of years; **km**, kilometer; **Ma**, millions of years

et al. 2019). This high-resolution chronostratigraphic framework at Corral Bluffs allows us to infer a reasonably precise age of the specimens described here—DMNH EPV.136181 and DMNH EPV.103990—relative to the K–Pg boundary.

DMNH EPV.136181 consists of a laterally compressed cranium with both dentaries in occlusion and was preserved in a small phosphatic concretion, a mode of preservation that is typical of the exceptional vertebrate fossil remains at Corral Bluffs (Lyson et al. 2019). This specimen was not discovered in-situ, but it was collected on a flat with only ~4 m of outcrop above it (DMNH Loc. 18898). Thus, the stratigraphic position of DMNH EPV.136181 is between 97 and 101 m above the K–Pg boundary, yielding an estimated age of ca. 65.43 Ma, approximately 610 ka after the K–Pg boundary (Fig. 2; Gradstein et al. 2012; Lyson et al. 2019). Mammalian biostratigraphy at Corral Bluffs further indicates that this specimen falls within the upper portions of the Puercan 2 (Pu2) NALMA (Eberle 2003; Lyson et al. 2019).

A second specimen, DMNH EPV.103990 (previously identified as *Oxyacodon* sp.; Lyson et al. 2019), consists of a partial right dentary preserving a portion of m1 and nearly complete m2–3. DMNH EPV.103990 was not preserved in a phosphatic concretion, but rather was recovered from a vertebrate microfossil bonebed (sensu Rogers and Brady 2010; DMNH Loc. 6284), which has also yielded other mammalian (*Loxolophus* sp.), reptilian (*Hoplochelys*, *Compsemys*, baenid and trionychid turtles, *Champsosaurus*, and crocodilians), and gar fish fossils. DMNH Loc. 6284 is 97 m above the K–Pg boundary, yielding an estimated age of ca. 65.43 Ma, approximately 610 ka after the K–Pg boundary (Fig. 2; Gradstein et al. 2012; Lyson et al. 2019). Finally, mammalian biostratigraphy at Corral Bluffs indicates that this specimen falls within the late Pu2 NALMA (Lyson et al. 2019).

Materials and methods

Specimen DMNH EPV.136181 was collected by TRL in the winter of 2020, and DMNH EPV.103390 was collected by Denver Museum of Nature & Science volunteer Sharon Milito in the fall of 2016. Following manual preparation of DMNH EPV.136181, the specimen was scanned using the micro-computed tomography (μCT) facilities at the High-Resolution X-ray Computed Tomography Facility of the University of Texas at Austin with the following scan parameters: North Star Imaging scanner, Fein Focus High Power source, 90 kV, 0.14 mA, aluminum foil filter, Perkin Elmer detector, 0.5 pF gain, 1 fps, 1×1 binning, source to object=86.928 mm, source to detector=731.108 mm, voxel size=23.8 μm, total slices=1838.

Specimen DMNH EPV.103390 was scanned at the Shared Materials Instrumentation Facility (SMIF) at Duke University with the following scan parameters: Nikon XTH 225 ST, 165 kV, 90 uA, Perkin Elmer 1620 AN3 CS CT detector, source to object=56.880 mm, source to detector=737.964 mm, voxel size=15.4 μm, total slices=2300.

Manual segmentation, three-dimensional (3D) reconstructions, and measurements of the μCT data were performed using Avizo 2022.2 (Thermo Fischer Scientific). The 3D models of each well-preserved element were exported as Polygon File Format (PLY) files. All 3D models with scanning parameters are available at MorphoSource (www.morphosource.org/concern/parent/000603715/media/000603718); we encourage the reader to utilize these 3D models.

Dental terminology follows Archibald (1982), Nessov et al. (1998), and Kielan-Jaworowska et al. (2004). Lowercase letters (p and m) indicate lower premolars and molars and uppercase letters (P and M) indicate upper premolars and molars, respectively, with numbers increasing serially mesially to distally, and R and L to indicate whether the tooth was from the right or left side, respectively. Also, note that we refer to premolars as P/p1–4, not P/p1–2 and P/p4–5 premolar homologies. Dental measurements follow Archibald (1982) and Lillegraven and Bieber (1986) and were taken in occlusal view using the 'Measure' tool in Avizo. Tooth-length measurements represent maximum mesiodistal length; tooth-width measurements represent maximum buccolingual width. Cranial terminology follows Wible et al. (2009) and Wible (2011).

Body mass was estimated based on the crown area (X) of the lower first molar measured as mesiodistal length * maximum buccolingual width using the following regression equations of Legendre (1986): (1) All mammals: ln (body mass)=1.827*ln(X)+1.810; (2) Small mammals (<500 g): ln (body mass)=1.621*ln(X)+1.786.

Systematic paleontology

MAMMALIA Linnaeus, 1758
EUTHERIA Gill, 1872
?UNGULATA Linnaeus, 1758
PERIPTYCHIDAE Cope, 1882
CONACODONTINAE Archibald, Schoch, and Rigby, 1983

Militocodon gen. nov.

Etymology. In honor of Sharon Milito, for her dedication to paleontology and education in the Denver Basin and for finding referred specimen DMNH EPV.103390.

Type and only known species. *Militocodon lydae.*

Distribution. Puercan 2 of the Denver Formation, D1 Sequence at Corral Bluffs (El Paso County, Colorado).

Diagnosis. Resembling the Conacodontinae (sensu Archibald et al. 1983b) in: M1–3 hypocone large and lingually expanded; protocone absent on P3. Resembling *Oxyacodon* (sensu Archibald et al. 1983a) in: premolars slightly inflated but P/p4 shorter or subequal in length to M/m1; para- and metastylar lobes on M1–3 more buccally expanded than in *Alticonus*, *Ampliconus*, *Miniconus*, *Tinuviel*, *Anisonchus*, *Conacodon*, *Haploconus*, and *Hemithlaeus*; metacingulum continuous with metastylar region; paraconule absent with postparaconule wing meeting preprotocrista near apex of protocone; hypocone expanded lingually beyond the protocone; paraconid on p4 small, situated near the base of the crown; narrow buccal cingulid present on lower molars and lingual cingulid absent on lower premolars and molars. Differing from *Oxyacodon* in: greater expansion of para- and metastylar lobes on P4, with the former also projecting farther mesially; hypocone lingual face more vertically oriented on M2–3, not sloping prominently lingually; hypocone apex distinctly distal to protocone apex, especially on M2, resulting in a more rectangular (rather than triangular) occlusal outline; paraconid on m1–3 not closely appressed to metaconid, resulting in a mesiolingually open trigonid basin; trigonid taller relative to talonid, due in part to a taller protoconid.

Discussion. We interpret *Militocodon* as a basal conacodontine periptychid. Within Conacodontinae, the dentition of *Militocodon* is most like that of *Oxyacodon*; for example, it exhibits a lingually expanded hypocone, and the paraconule on the upper molars and the P3 protocone are both absent. Nonetheless, as articulated in the 'Diagnosis', *Militocodon* is morphologically distinct from all recognized species of *Oxyacodon*: *O. apiculatus*, *O. agapetillus*, *O. priscilla*, and *O. ferronensis* (Archibald et al. 1983a). Two other putative species of *Oxyacodon*, *O. marshater* and *O. josephi*, are not considered here because *O. marshater* was only tentatively retained in *Oxyacodon* (Archibald et al. 1983a) and there is debate about whether *O. josephi* is a valid species of *Oxyacodon* (for discussion, see Archibald et al. 1983a vs. Shelley 2018). The diagnosis for *Oxyacodon* was revised to differentiate it from more basal periptychids (i.e., *Mimatuta*) and the more derived *Conacodon* (Archibald et al. 1983a); as such, *Militocodon* presents a challenging taxonomic problem. Because *Militocodon* and *Oxyacodon* are both morphologically derived relative to taxa like *Mimatuta* and *Maiorana* but more plesiomorphic than *Conacodon*, many of the dental characteristics exhibited by *Militocodon* fit the diagnosis for *Oxyacodon*. Nonetheless, *Militocodon* exhibits more plesiomorphic dental characteristics than all species of *Oxyacodon*.

That the dentition of *Militocodon* is distinct and plesiomorphic relative to *Oxyacodon* is evident in its morphological similarity to the putatively basal periptychids *Maiorana* and *Mimatuta*. Like *Maiorana* (especially specimens of *M. noctiluca* from the Great Divide Basin; e.g., Atteberry and Eberle 2021), the lower molars of *Militocodon* have taller trigonids relative to the talonids and have primary cusps that are not as appressed compared to *Oxyacodon* (especially apparent in the lack of appression between the paraconid and metaconid). Like *Mimatuta minuial* (especially the holotype, YPM-PU 14211), the para- and metastylar lobes on P4 are more prominent in *Militocodon*, although they are oriented mesiodistally (like *Oxyacodon*) rather than flaring buccally, and the hypocone is distinctly distal to the protocone apex (especially on M2). There are other plesiomorphic features (e.g., Bown and Kraus 1979) in the dentition of *Militocodon* that are distinctive relative to most, but not all, specimens of *Oxyacodon*. For example, compared to most specimens of *Oxyacodon*, the para- and metastylar lobes on M1–2 of *Militocodon* are more prominent, exhibit buccolingually broad stylar shelves between the ectocingulum and paracone and metacone, respectively, and extend buccally to form a pronounced ectoflexus. Also, the entoconids and hypoconulids of *Militocodon* are less inflated, resulting in relatively broad talonid basins. These presumably plesiomorphic aspects of the dentition of *Militocodon* do overlap with the range of variation exhibited by some *Oxyacodon* spp. (especially *O. apiculatus*; see, for example, Archibald et al. 1983a: Fig. 1), so they are not diagnostic by themselves. Nonetheless, taken together, the suite of plesiomorphies exhibited in the dentition of *Militocodon* make it distinct from *Oxyacodon*.

The holotype of *Miniconus archibaldi* (formerly *Oxyacodon archibaldi*; Atteberry and Eberle 2021), a fragmentary right maxilla with partial P3–M3 (Middleton and Dewar 2004), also resembles *Militocodon*; in particular, its hypocones are similar in size and position. Yet, the para- and metastylar regions on the M1–M3 of *Militocodon* are expanded buccally with a pronounced ectoflexus, whereas they comprise little more than the ectocingulum on *M. archibaldi*. Further, the hypocone projects farther lingually and is well separated from the protocone by a broad postcingulum shelf in *Militocodon*, whereas it projects just past the lingual border of the protocone and more closely adheres to the distal face of the protocone in *M. archibaldi*. In those respects, the upper molars of *Miniconus* more closely resemble those of *Ampliconus*, *Alticonus*, and *Tinuviel*.

Militocodon lydae sp. nov.

Etymology. In honor of Lyda Hill, a longtime champion of Colorado Springs and key supporter of post-K–Pg

recovery research at the Denver Museum of Nature & Science.

Holotype. DMNH EPV.136181, partial skull, including posterior maxillae and dentaries, RP/p4–M/m3 and LP/p3–M/m3, and partial neuro- and basicranium.

Type locality and age. The holotype specimen is from DMNH Loc. 18898 in the Corral Bluffs study area. The Corral Bluffs study area is situated east of Colorado Springs, El Paso County, Colorado (Fig. 2) in the southern Denver Basin. The type locality is located in the Denver Formation, Danian, lower Paleocene. Biostratigraphically, the holotype occurs in the late Puercan 2 NALMA and within pollen zone 2 (Fig. 2).

Referred material. DMNH EPV.103390 (DMNH Loc. 6284), right partial dentary m1 fragment and m2–3. Three-dimensional models of this specimen, as well as of the holotype specimen, are available at MorphoSource (www.morphosource.org/concern/parent/000603715/media/000603718).

Referred material age. Same as for holotype.

Distribution. Same as for genus.

Diagnosis. Same as for genus.

Descriptions

The holotype (DMNH EPV.136181) is a partial skull (Fig. 3); the posterior portions of both maxillae and dentaries are preserved with the upper and lower cheek teeth in approximate occlusion, including LP3–LM3, RP4–RM3, Lp3–Lm3, and Rp4–Rm3. DMNH EPV.103390 is a dentigerous lower right jaw fragment preserving a portion of m1 and nearly complete m2–3 that we assign to *Militocodon lydae* although we note several differences, notably size, that are listed below in our descriptions. We encourage the reader

to utilize the 3D models of these specimens (www.morphosource.org/concern/biological_specimens/000603687) in conjunction with the description and 2D figures. In DMNH EPV.136181, a partial C1 (atlas) vertebra is also preserved, tucked beneath the posteroventral portion of the skull. Most of the rostrum is broken away due to erosional damage, the skull is strongly compressed mediolaterally, there is moderate plastic deformation especially of the dorsal margin, and the posterior portion of the skull is substantially crushed and distorted. A large crack runs posterodorsally through the entirety of the specimen from the base of the dentary below Lm1 and Rm2 to the approximate anteroposterior midline on the dorsal margin. The cranial bones are patchily preserved and brecciated in many places, obscuring many of their sutural contacts. Nonetheless, portions of the maxillae, jugals, lacrimals, frontals, parietals, sphenoid complex, right squamosal, and petrosals are preserved.

Overall, the portion of the skull that is preserved is oval-shaped in lateral views, with the long-axis oriented anteroposteriorly. Although they are cracked and exhibit moderate plastic deformation, the zygoma are relatively gracile, decreasing in dorsoventral height posteriorly towards the glenoid fossa. Below, we describe the preserved teeth, dentaries, and cranial bones in detail.

Dental descriptions

Third lower premolar (p3; Fig. 4a, c, d). Specimen DMNH EPV.136181 preserves only a partial Lp3, with the mesial portion of the crown to near the apex of the protoconid and most of the mesial root broken away, along with moderate apical wear on the distolingual portion of the protoconid. Despite the damage to the mesial portion of the tooth, p3 is double-rooted, ovoid in occlusal outline, the protoconid height is apparently shorter than that of p4 but subequal to
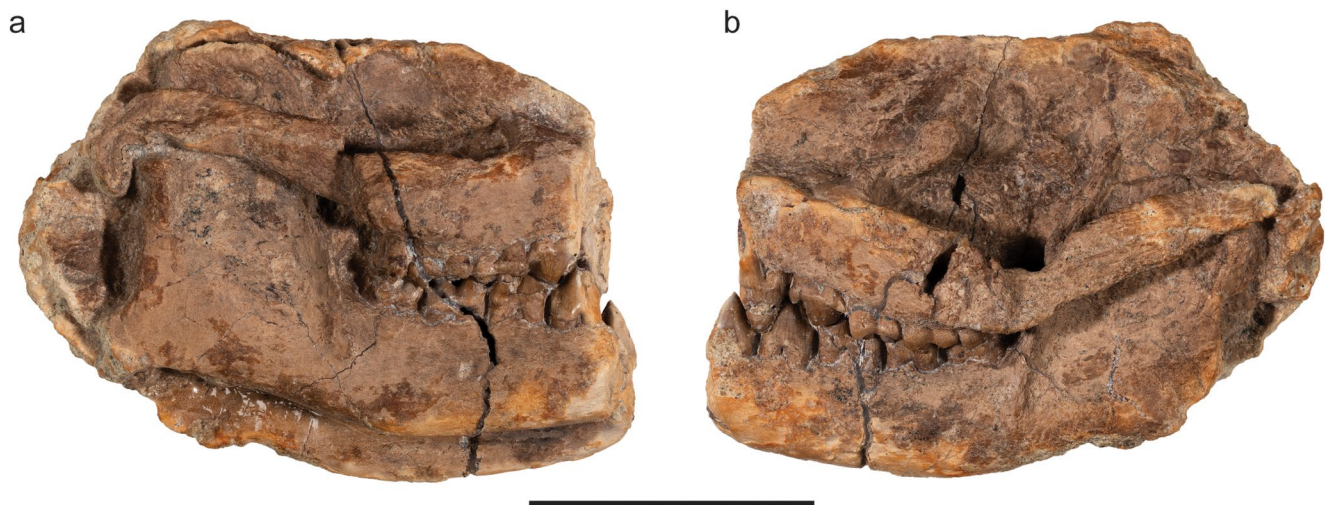
a

b

Fig. 3 Holotype of *Militocodon lydae* gen. et sp. nov. (DMNH EPV.136181) in right (**a**) and left (**b**) lateral views. Scale bar equals 2 cm
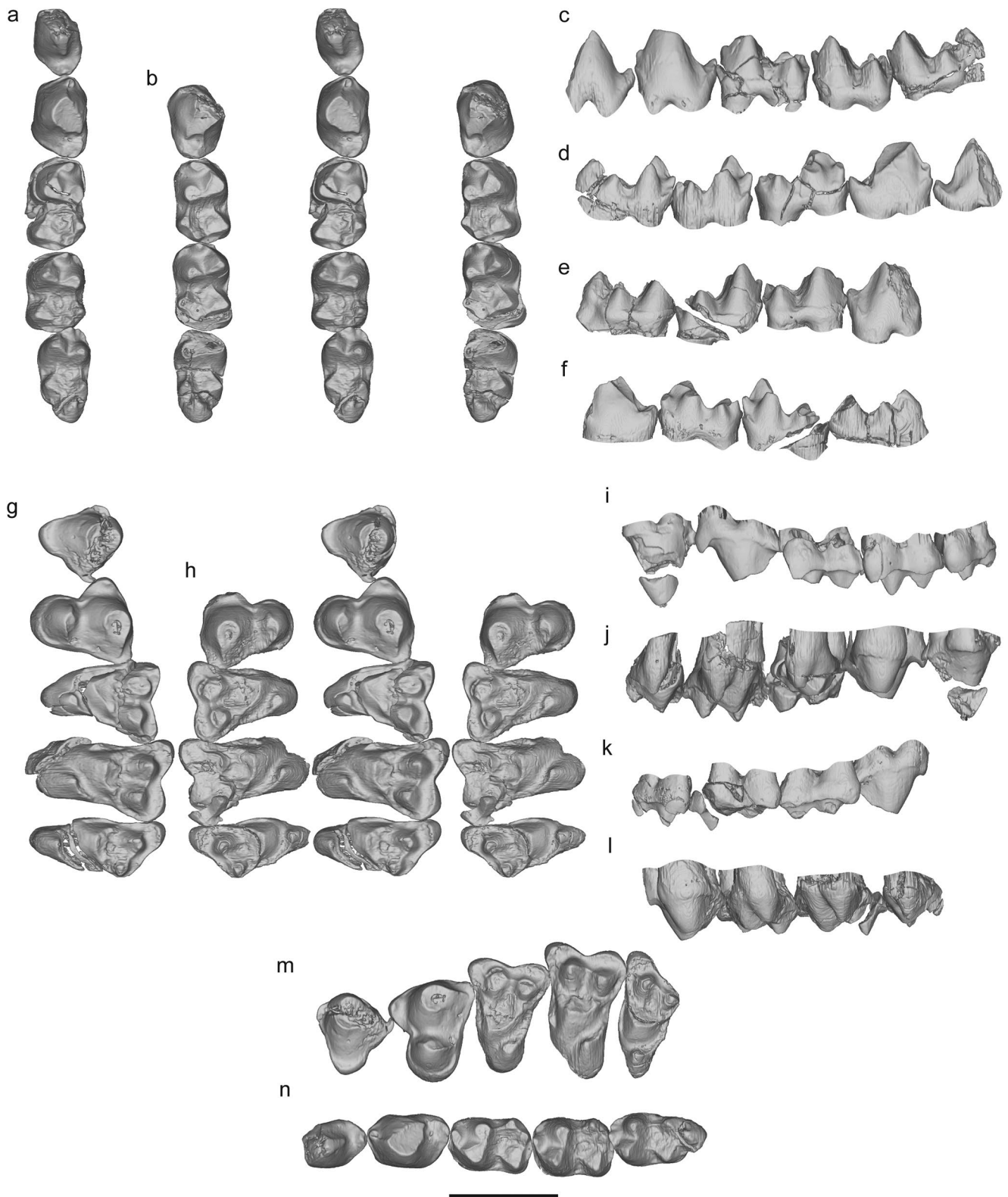
Fig. 4 Dentition of the holotype of *Militocodon lydae* gen. et sp. nov. (DMNH EPV.136181). Left p3 (partial) through m3, right p4 (partial) through m3, left P3 through M3, and right P4 through M3 in stereo occlusal (**a**, **b**, **g**, **h**), buccal (**c**, **e**, **i**, **k**), and lingual (**d**, **f**, **j**, **l**) views, respectively. **m** and **n**. Composite upper and lower tooth rows assembled from the best-preserved teeth. Note that the crenulations apparent on the basal portions of some teeth are artifacts from segmentation of the µCT data. Scale bar equals 5 mm

that of m1–3, apex projects dorsally, buccal face is inflated and convex, lingual face slightly concave, and postvallid, the distal wall of the trigonid, is buccolingually narrow, resembling a nearly vertically oriented isosceles triangle with its apex meeting the distolingual wear facet of the protoconid and the base meeting at the talonid heel. Given the damage to the tooth, it is uncertain whether a paraconid was present, but given that the lingual face of the protoconid appears uninterrupted to its apex, we interpret that the metaconid was absent. The distal portion of the crown is mesiodistally narrow, roughly crescentic in occlusal view, and saddle-like, with the buccal and lingual portions sloping ventrally away from its midline and the distal portion rising to form a broad, cone-like talonid heel with its apex situated at the midline of the tooth and reaching the height of the precingulid of p4. The talonid heel consists of one central cusp situated at the apex of the distal talonid with what might have been a smaller, distolingual cuspule that connects to a narrow ridge that descends mesioventrally to form a low distolingual border of the talonid. The distal face of the talonid heel exhibits a small, shallow, ovoid depression immediately ventral to the twinned cuspules, but is otherwise smooth and gently convex. Measurements: Length = 3.5 mm (estimate), Width = 2.24 mm.

Fourth lower premolar (p4; Fig. 4a–f). DMNH EPV.136181 preserves both p4s. Lp4 is complete but exhibits substantial apical wear on the trigonid, and much of the mesial half of Rp4 is missing due to postmortem damage and there is substantial apical wear on the trigonid; as such, the foregoing description is primarily based on Lp4. p4 is double-rooted and ovoid in occlusal outline. The mesial face of p4 exhibits a mesiodistally short precingulid that projects only slightly on the mesiobuccal and mesiolingual faces of the crown before tapering off distoventrally on both sides. The paraconid is small, conical, dorsal to the precingulid, slightly lingual to the midline of the tooth, exhibits moderate apical wear, and is connected to the protoconid by a narrow paracristid. Although it exhibits substantial apical wear, the protoconid is likely the tallest cusp in the p3–m3 row, has a dorsally projecting apex, a convex mesial face with a paracristid that is slightly lingual to the midline of the tooth and descends steeply mesially to the paraconid, and inflated and convex buccal and lingual faces. The postvallid is oriented mesiobuccally and bisected by a narrow ridge situated along the midline of the tooth that descends steeply distally to meet the cristid obliqua. Lingual to that ridge, the postvallid is slightly concave, nearly vertically oriented, and met ventrally by a small talonid basin, but buccal to that ridge, the postvallid consists of a broad, shallow hypoflexid that faces distobuccally and descends more gently buccoventrally past the talonid basin and exhibits a prominent triangular wear facet. The talonid is mesiodistally short,

semicircular in occlusal view, and strongly asymmetrical on the buccal versus lingual side. The lingual side of the talonid includes a small talonid basin, bordered buccally by the broad cristid obliqua and lingually by a sharp, narrow entocristid that extends to the raised distal portion of the talonid (potentially the hypoconid). Measurements: Length = 3.82 mm, Width = 2.53 mm.

First lower molar (m1; Fig. 4a–f). DMNH EPV.136181 preserves both Lm1 and Rm1, and DMNH EPV.103390 preserves only the distal root and a broken portion of the Rm1 talonid. Both molars exhibit moderate apical wear, but Lm1 is substantially brecciated; as such, the foregoing description is primarily based on Rm1. m1 is double-rooted and the crown is rectangular in outline. The mesial face of the crown exhibits a mesiodistally short and faint precingulid that runs buccolingually below the base of the paraconid and connects to the narrow buccal cingulid. The protoconid is the largest cusp of the trigonid in circumference and possibly height, followed by the metaconid then the paraconid. The paraconid is worn but is clearly situated at the approximate midline of the tooth and projects slightly mesially. The paracristid rises steeply from the distobuccal face of the paraconid forming a mesiobuccally convex arc that ascends the mesial face of the protoconid. Although worn, the apex of the protoconid was likely much taller than that of the metaconid or paraconid. The protoconid is positioned slightly mesial to the metaconid, and the paraconid is widely separated from the metaconid, such that the trigonid basin is open mesiolingually. Both the protoconid and metaconid apices were apparently separated and likely formed a protocristid notch, but both of those features are obscured by apical wear. Overall, the trigonid is taller than the talonid, moderately inflated, convex buccally, steeply sloped lingually, with a nearly vertical postvallid, and the apices of the trigonid cusps were not closely appressed, forming a relatively large trigonid basin. The hypoflexid is mesiodistally narrow dorsally and broadens ventrally, forming a shallow platform between the distobuccal margin of the trigonid and mesiobuccal margin of the talonid.

The hypoconid is by far the largest cusp of the talonid in circumference, followed by the entoconid then hypoconulid. The hypoconid is mostly conical, but wear accentuates a flat, triangular mesiolingual face that broadens as it descends into the talonid basin. The hypoconid is bordered mesiobuccally by the cristid obliqua, the mesiolingual extent of which is centered below the midpoint of the protoconid, and distobuccally by the buccal part of the postcristid that descends to form an oblique notch between the hypoconid and hypoconulid when observed in distal view. Distoventral to that notch is a distinct postcingulid. The hypoconulid is situated slightly distal to the hypoconid, is roughly conical, and is more closely positioned to the slightly larger in

circumference entoconid, connected by a narrow and tall lingual part of the postcristid, and has a vertical distal wall. The entoconid is positioned mesially relative to the hypoconid, is roughly conical, and exhibits a prominent entocristid that climbs the postvallid just lingual to the midpoint of the metaconid in distal view and encloses the talonid basin in lingual view. Overall, the talonid basin is broad and the talonid slightly exceeds the buccolingual width of the trigonid. Measurements (Rm1): Length=3.98 mm, Width=2.66 mm.

Second lower molar (m2; Fig. 4a–f). DMNH EPV.136181 preserves Lm2 and Rm2, and DMNH EPV.103390 preserves Rm2 (Fig. 5), all of which exhibit slight apical wear. The trigonids of all molars are well preserved, but a crack is running dorsodistally to ventromesially through the base of the crown on Rm2 of DMNH EPV.136181 and a broken entoconid on the Rm2 of DMNH EPV.103390 obscures the lingualmost portion of the talonid; as such, the foregoing description is mostly based on Lm2 of DMNH 136181 when discussing the morphology of the talonid. m2 is double-rooted and is generally very similar to that of m1, with the following exceptions: (1) m2 is slightly shorter relative to the width and the trigonid and talonid are more similar in width, (2) there is a cuspule on the mesiolingual ridge descending from the paraconid, (3) the hypoconulid is more closely twinned with the entoconid, and (4) the talonid basin is not as enclosed by the entocristid. Note that we avoid the term 'parastylid' to refer to the cuspule on the mesiolingual ridge descending from the paraconid because it is not a distinct cusp like those parastylids identified in other periptychids (i.e., *Miniconus*; Atteberry and Eberle 2021). Measurements: DMNH EPV.136181 Lm2: Length=3.69 mm, Width=2.68 mm; DMNH 103390 Rm2: Length=3.11 mm, Width=2.56 mm.

Third lower molar (m3; Fig. 4a–f). DMNH EPV.136181 preserves Lm3 and Rm3. On Lm3, a small crack has slightly displaced the hypoconulid distolingually, and on Rm3, there is substantial breakage to the trigonid apices and two small buccolingually oriented cracks that slightly distally displace

the talonid from the trigonid and the hypoconulid from the talonid. DMNH EPV.103390 preserves a nearly complete Rm3 (Fig. 5) that is missing a small portion of the distal hypoconulid. The foregoing description is based primarily on the Lm3 of DMNH EPV.136181. m3 is double-rooted and the size, shape, and orientation of the trigonid cusps are very similar to those on m2. However, the distolingually descending ridge from the base of the paraconid on m3 is more prominent and hosts two cuspules, with the more dorsal cuspule abutting the paraconid being slightly larger than the more ventral cuspule. When observed in occlusolingual view, these ridge-hosted cuspules in combination with the paraconid and protoconid form a mesiobuccally convex arc of cusps of decreasing size, moving from the protoconid to paraconid then dorsal cuspule to ventral cuspule.

The hypoconulid is by far the largest cusp of the talonid in both circumference and height, followed by the hypoconid then entoconid. The morphology of the hypoflexid, cristid obliqua, hypoconid, entoconid, and entocristid closely resemble those of m1 (including an enclosed talonid basin); however, the entoconid is positioned slightly distal to the hypoconid (rather than slightly mesial to that cusp as in m1 and m2). Also, on the Rm3 of DMNH EPV.103390, the entocristid descends mesiolingually past the metaconid rather than contacting its distal face as in DMNH EPV.136181. The hypoconulid forms a distinct distal lobe, and the hypoconulid apex is slightly recurved mesially and approaches the height of the protocristid notch. As in m1 and m2, a steep postcristid connects the hypoconulid to the entoconid, closing off that portion of the talonid basin, but ventral to that ridge on m3 is a lingually expanded shelf that extends from the base of the entoconid to near the apex of the hypoconulid. The hypoconulid remains separated from the hypoconid by a broad triangular groove that broadens distoventrally and opens the talonid basin. Measurements: DMNH EPV.136181 Rm3: Length=4.34 mm, Width=2.53 mm; DMNH 103390 Rm3: Length=3.81 mm, Width=2.37.
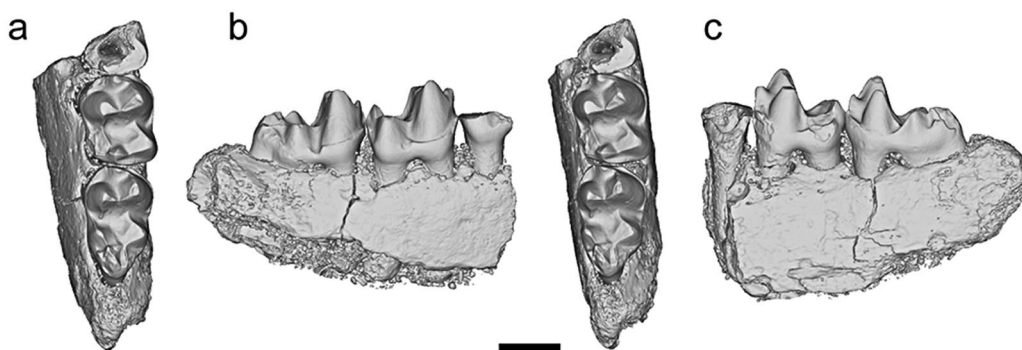

Fig. 5 A second specimen of *Militocodon lydae* gen. et sp. nov. (DMNH EPV.103390), represented by a right m1 fragment and m2–3, in stereo occlusal (**a**), buccal (**b**), and lingual (**c**) views. Scale bar equals 2 mm

Third upper premolar (P3; Fig. 4g, i, j). DMNH EPV.136181 preserves only LP3, which is mostly intact except for a crack that has separated the apex of the paracone from the rest of the crown. P3 has three roots that are subequal in size. The crown is the smallest preserved in the upper tooth row, is slightly inflated, and roughly triangular in occlusal outline, with slight mesiodistal waisting near the lingual base of the paracone. The parastyle is reduced, forming a small, crescentic, mesiobuccal projection from the base of the paracone, and does not host any cuspules. The paracone makes up the majority of the occlusal breadth of the crown, is tall and roughly conical, and its buccal margin is not bordered by a distinct buccal cingulum. The preparacrista is absent but the distal face of the paracone is too fragmentary to determine the presence or absence of a postparacrista. There is no protocone; instead, a lingual cingulum continues along the base of a small protocone lobe. The metastyle is morphologically similar to the parastyle but projects slightly farther distally and is slightly narrower buccolingually. Measurements: Length = 3.77 mm, Width = 3.38 mm.

Fourth upper premolar (P4; Fig. 4g–l). DMNH EPV.136181 preserves both LP4 and RP4, both of which exhibit moderate attritional wear on the paracone and protocone, and the mesial portion of the parastyle is broken away on RP4. As such, the foregoing description is based primarily on LP4. P4 has three roots in which the root supporting the protocone is the largest in circumference, followed by the mesiobuccal root then the distobuccal root. The crown is inflated, approximately 1/3 times larger in coronal dimensions than P3, due mostly to the presence of a protocone and more prominently flaring parastylar lobe, and is subequal in length to M1 but narrower in width. In occlusal outline the crown is roughly trapezoidal, with a longer buccal margin than lingual, except for a pronounced flexure lingual to the parastylar lobe. The parastyle is estimated to be approximately 25% the height of the paracone, and it is positioned on a prominent parastylar lobe that flares mesially and forms a saddle-shaped, basin-like parastylar groove between the parastyle and paracone. The paracone is by far the largest cusp in circumference and height on P4 and was likely the tallest cusp in the upper tooth row (this is obscured by wear). It is roughly conical, separated from the protocone by a buccolingually broad, saddle-like groove, and exhibits no preparacrista but possesses a worn but likely prominent postparacrista that descended from its apex to the metastylar lobe. The protocone is mesiodistally longer than its buccolingual width and much shorter than the paracone (at least half its height). Near the buccolingual midline of the protocone runs a preprotocrista that descends from its apex mesiobuccally and then buccally to form a mesiodistally narrow and shallow basin between it and the saddle

between the paracone and protocone. A prominent cingulum wraps around the lingual base of the protocone. The metastylar lobe is morphologically similar to the parastylar lobe but is smaller in width, flares distobuccally, is narrower buccolingually, does not host a cuspule, and is bisected by the postparacrista descending from the distal face of the paracone. Two ridges descend from the metastylar lobe apex; one trending mesiobuccally to meet the ectocingulum, and one trending mesiolingually to form a shallow groove between the metastyle and the paracone. The ectocingulum is most visible on its mesial and distal extents where it meets the para- and metastylar lobes, respectively; it is little more than a faint ridge buccal to the paracone. Measurements: Length = 3.96 mm, Width = 4.50 mm.

First upper molar (M1; Fig. 4g–l). DMNH EPV.136181 preserves both LM1 and RM1, both show moderate attritional wear on the paracone, metacone, and hypocone, and LM1 is substantially cracked, separating the buccal, middle, and lingual thirds of the tooth from one another. Thus, the foregoing description is based primarily on RM1. M1 has three roots in which the lingual root that supports the protocone and hypocone is the largest in circumference, followed by the mesiobuccal root then the distobuccal root. The crown is roughly heart-shaped in occlusal outline due to its ectoflexus, mesio- and distobuccally flaring para- and metastylar regions, respectively, and the overall tapering in the mesiodistal length of the crown from the buccal margin to the lingualmost edge of the hypocone. The buccal margin, as traced by the ectocingulum, is slightly asymmetrical: the deepest part of the ectoflexus is just mesial to the centrocrista notch, and the parastylar region is expanded more mesially while the metastylar region is positioned slightly more buccally. The para- and metastylar lobes project buccally and form a shallowly basined stylar shelf between the ectocingulum, preparacrista, paracone, centrocrista, metacone, and postmetacrista, but that basin narrows to little more than the ectocingulum buccal to the buccalmost edge of the paracone. The paracone is positioned slightly buccally relative to the metacone, both are similar in mesiodistal length, but whereas the metacone is roughly symmetrical in coronal dimensions the paracone is wider buccolingually; whether the paracone was also taller than the metacone is obscured due to wear. The bases of the para- and metacone are separated. The weak preparacrista is short, steeply descends (likely from the apex when unworn) the mesial face of the paracone, then curves buccally to meet the parastyle on the rounded parastylar lobe. The stronger postmetacrista shallowly descends (likely from the apex when unworn) straight along the distobuccal face of the metacone to meet the slight metastyle on the metastylar lobe. Breakage and wear obscure the relative height of the para- and metastyle to the paracone or to each other, although the parastyle appears to

be taller than the metastyle. A weak centrocrista is present (most visible on the RM1) created by the faint postparacrista on the distal face of the paracone and faint premetacrista on the mesial face of the metacone. The paraconule is absent; instead, the faint remnant of preparaconule crista meets, just mesiolingual to the lingual margin of the paracone, an uninterrupted distolingual-to-mesiobuccal-trending ridge formed by the preprotocrista and preparaconule crista. The metaconule is small, little more than a swelling of enamel just lingual to the lingual margin of the metacone, with no obvious premetaconule crista (potentially obscured due to wear), and a postmetaconule crista that extends distobuccally to form a metacingulum that terminates at the junction between the postmetacrista and ectocingulum at the distalmost margin of the crown. The trigon basin is deep, buccolingually wide, but still fairly long mesiodistally in part due to the lack of postparaconule and premetaconule cristae encroaching on the basin. Although exhibiting apical wear, the protocone was likely similar in height to the para- and metacones; however, it has a much greater circumference and girth than the other primary cusps. The apex of the protocone is slightly positioned buccally but is distinctly positioned mesially to be in buccolingual line with the paracone. The mesiolingual face of the protocone is rounded and slopes steeply to form the mesiolingual base of the crown. The precingulum forms a mesiodistally short shelf that extends from the level just buccal to the protocone apex to the lingual edge of the paracone. The distolingual hypocone is the most prominent cusp; it extends lingually past the apex of the protocone to form the majority of the lingual margin of the crown, and is in buccolingual line with the metacone. The hypocone is well separated from the protocone and postprotocrista with no prehypocrista. On the distobuccal face of the hypocone, a strong posthypocrista runs buccally to join the postcingulum that then terminates distal to the position of the metaconule. The postcingulum is narrowest near the level of the metaconule then broadens lingually toward the hypocone, forming a mesiodistally broad shelf between the hypocone and the protocone. The lingual margin of the hypocone is inflated and convex, but is relatively steep, sloping slightly lingually. Measurements (RM1): Length = 3.86 mm, Width = 5.00 mm.

Second upper molar (M2; Fig. 4g–l). DMNH EPV.136181 preserves both LM2 and RM2; LM2 is in excellent condition, with only a crack near the base of the crown separating a mesial portion of the lingual root from the rest of the tooth and slight attritional wear on the distal face of the paracone, whereas the buccal portion of RM2 is damaged, with most of the paracone missing and the most of the metacone and metastylar region cracked away from the rest of the crown. As such, the foregoing description is based primarily on LM2. M2 has three roots in which the lingual root that supports the hypocone and protocone is the largest in circumference, followed by the mesiobuccal root and the distobuccal root. M2 is the largest in the preserved upper tooth row, and its crown is broadly similar to that of M1 but there are a number of notable differences. The buccal margin, as traced by the ectocingulum, is more strongly asymmetrical: the parastylar region is much narrower than the metastylar region, and both the para- and metastylar regions flare more prominently buccally to form a broader stylar shelf and more pronounced ectoflexus, the deepest point of which is shifted mesially to be in buccolingual line with the distal margin of the paracone. The paracone is likely slightly taller than the metacone (but the apices of the paracone and metacone of M1 are not preserved), and both cusps are similar in coronal dimensions except the buccal face of the paracone is convex and approaches the ectoflexus, whereas on the metacone it is relatively flat, nearly flush with the pre- and postmetacristae descending from its apex. The mesial face of the paracone is rounded and convex, as is the distal face of the metacone, but the distal face of the paracone and mesial face of the metacone are relatively flat as they open into the trigon basin. As in M1, the paraconule is absent and the preparaconule crista and preprotocrista meet to form the paracingulum from the protocone apex to the near the level of the buccal termination of the precingulum; however, the postparaconule crista is more pronounced, extending from the lingual base of the paracone to meet the preprotocrista near the apex of the protocone. The metaconule is also more pronounced than that in M1, with a short premetaconule crista that terminates after a short distance and a postmetaconule crista that extends distobuccally to join with the metacingulum which, in turn, merges with the ectocingulum near the junction with the postmetacrista. The trigon basin is smaller in coronal dimensions than that in M1 due primarily to the protocone apex being positioned farther buccally and the lingual face of the protocone sloping more prominently lingually. The precingulum is generally similar to that in M1, but in M2 it exhibits a swelling of enamel near its lingual terminus (potentially an incipient protostyle) and extends farther buccally, joining to form an uninterrupted ridge with the paracingulum and ectocingulum around the mesiobuccal portion of the crown. The hypocone is also larger and its base extends farther lingually in M2 than in M1, but in both molars the hypocone apex is positioned in buccolingual line with the apex of the metacone. Measurements (LM2): Length = 3.76 mm, Width = 5.99 mm.

Third upper molar (M3; Fig. 4g–l). DMNH EPV.136181 preserves both LM3 and RM3 and both are relatively complete with only minor attritional wear on their paracones and protocones; however, the hypocone on LM3 has been slightly cracked away from the rest of the crown. As such, the foregoing description is based primarily on RM3. M3

has three roots in which the lingual root supports the protocone and hypocone and is the largest in circumference, followed by the mesiobuccal root and the distobuccal root. M3 is mesiodistally short relative to the other molars but is similarly as transverse as M2. The buccal margin, as traced by the ectocingulum, is highly asymmetrical: the parastylar region flares prominently buccally, forming a broad parastylar basin around the paracone, whereas the metastylar region is nearly absent, forming a nearly straight-line trending distolingually from the midline of the paracone to the distal margin of the metacone, deviating only slightly with a very shallow ectoflexus just buccal to the distobuccal margin of the paracone. As in the other upper molars, the parastyle is strongly developed, but the M3 differs in that the metastyle is absent. The overall shapes of the paracone and metacone are similar to those on M2, but on M3 the metacone is much shorter and smaller in coronal dimensions than the paracone. As in the other upper molars, a short preparacrista descends the mesial face mesiobuccally from the apex of the paracone to cross the stylar shelf and join the ectocingulum, but no postmetacrista is present on the metacone, the distal face of which directly abuts the ectocingulum. The size, shape, and position of the metaconule, associated cristae, trigon basin, protocone apex, and the lingual face of the protocone all closely resemble those in M1; however, as in M2, the merged preparaconule crista and preprotocrista extend mesiobuccally to join the paracingulum and ectocingulum. The precingulum on M3 is slightly narrower mesiodistally but otherwise morphologically similar to that on M2. The postcingulum shelf and coronal dimensions of the hypocone itself are smaller than in the other molars, and the hypocone is positioned farther mesially, nearly in buccolingual line with the centrocrista notch. Measurements (RM3): Length = 2.84 mm, Width = 5.82 mm.
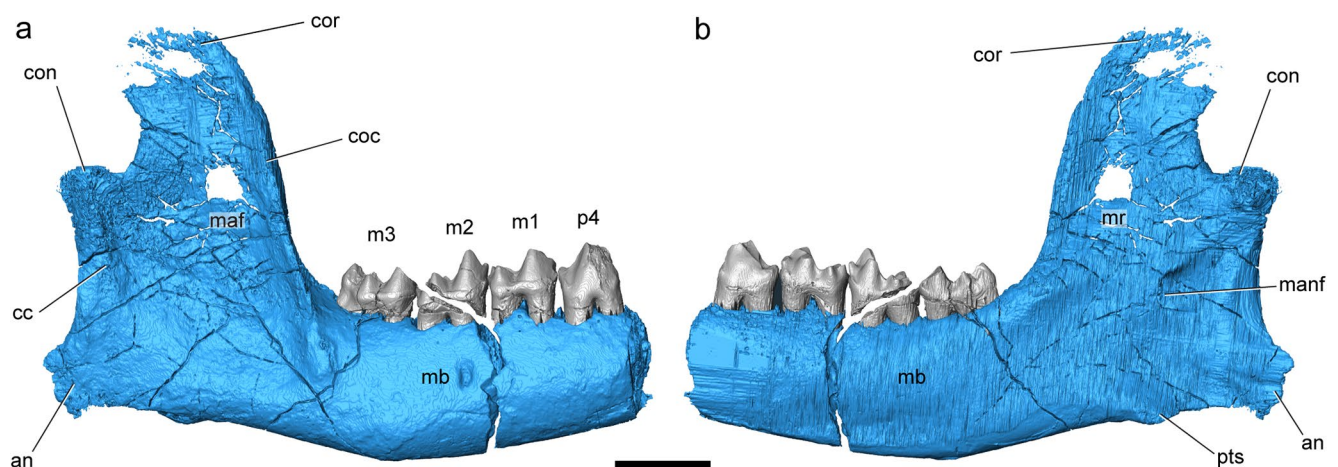
Skull descriptions

Dentary. The partial dentaries of DMNH EPV.136181 do not preserve the mandibular body rostral to p4 on the right side and rostral to p3 on the left side. Both dentaries are also missing the caudoventral aspects of the angular process. The right dentary is better preserved overall and preserves more of the mandibular ramus, including the mandibular condyle and coronoid process (Fig. 6), whereas the left dentary is missing most of these features, but preserves the location of a mental foramen on the mandibular body (Fig. 7).

Although incomplete, the mandibular body of DMNH EPV.136181 is not very deep and is dorsoventrally deepest ventral to the m3 trigonid and tapers rostrally from this point. On the lateral surface (visible only on the left dentary), there is an oval-shaped mental foramen (maximum length = 1.27 mm; length perpendicular to maximum length = 0.40 mm) ventral to the p3 for transmission of the mental nerve, artery, and vein (Fig. 7) (Wible 2011). In medial view, no mylohyoid line is identified, but there is a distinct trough on the ventral border of the body from the position of the m1 talonid to the m3 trigonid. DMNH EPV.136181 exhibits a small retromolar space caudal to the m3.

In comparison with the mandibular body, the mandibular ramus is relatively tall and extends far dorsally above the alveolar margin. Following the method of Shelley et al. (2018), the maximum dorsoventral height of the mandibular body divided by the maximum dorsoventral height of the mandibular ramus equals 0.37. The right mandibular ramus preserves portions of all three main processes: the coronoid process, the angular process, and the condylar process. The coronoid process extends dorsally, beyond the condylar process, and recurves slightly at its dorsal extent. At the rostral

Fig. 6 3D model of the right dentary of *Militocodon lydae* gen. et sp. nov. (DMNH EVP.136181) in buccal view (**a**) and lingual view (**b**). Abbreviations: **an**, angular process; **cc**, condyloid crest; **coc**, coronoid crest; **con**, mandibular condyle; **cor**, coronoid process; **maf**, masseteric fossa; **manf**, mandibular foramen; **mb**, mandibular body; **mr**, mandibular ramus; **m1**, first lower molar; **m2**, second lower molar; **m3**, third lower molar; **p4**, fourth lower premolar; **pts**, pterygoid shelf. Scale bar equals 5 mm
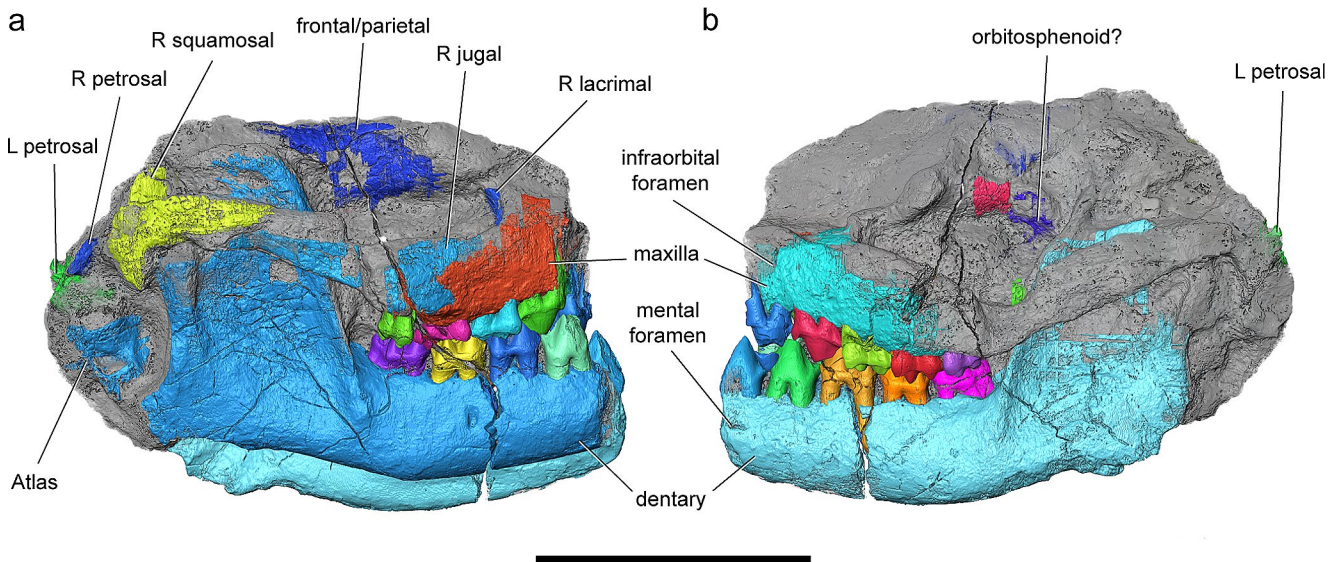
Fig. 7 3D rendering of the skull of *Militocodon lydae* gen. et sp. nov. (DMNH EVP.136181) with segmented 3D models of cranial bones shown in color in right (**a**) and left (**b**) lateral views. Scale bar equals 2 cm

aspect of the coronoid process is the coronoid crest which extends across the dorsoventral height of the coronoid process and continues ventrally onto the body of the mandible to roughly half the dorsoventral depth. The angle between the coronoid process and the alveolar margin of the body of the mandible is ~107°. Anteriorly defined by the coronoid crest and posteriorly defined by the condyloid crest of the condylar process is a shallow masseteric fossa which serves as the attachment site for the deep masseter. The ventral margin of this fossa is not well-defined, but it appears that the rostroventral extent of the masseteric fossa is at the level of the caudal root of the m3.

The condylar process of the mandibular ramus, which lacks a neck, is roughly half of the height of the coronoid process. In lateral view, the condyloid crest is visible as a raised ridge and defines the caudal boundary of the masseteric fossa. Continuous with the condyloid crest dorsally is the articular surface of the condylar process which articulates with the glenoid fossa of the squamosal and is positioned roughly the length of a molar dorsal to the occlusal plane. The articular surface is mediolaterally wider than it is dorsoventrally deep and is nearly flat on its dorsal surface. Extending caudoventrally from the mandibular ramus is the angular process, but this process is missing its distal extent on both sides with only parts of the pterygoid shelf preserved on the medial surface. This process was likely a narrow hook-like caudoventral extension based on the proximal remains, which are not wide and expanded. Dorsal to the angular process on the medial surface is a large mandibular foramen, which is roughly at the level of the occlusal plane. Caudal to the mandibular foramen is a short but defined fossa that leads into mandibular foramen.

Maxilla. DMNH EPV.136181 partially preserves both left and right maxillae, which contribute to the hard palate, lateral wall of the rostrum, and orbital floor. The right maxilla is better preserved (Figs. 7 and 8) and will serve as the basis for the following descriptions unless otherwise noted. Rostrally, the paired maxillae are broken at the level of P3 on the left side and at the level of P4 on the right side (Figs. 7 and 8). Preserved only on the left maxilla and dorsal to the caudal root of the P3 is a single infraorbital foramen that is oval with the long axis perpendicular to the rostrocaudal axis of the cranium (maximum diameter = 3.38 mm, diameter perpendicular to that = 1.23 mm). This foramen would transmit the infraorbital vessels and nerve (cranial nerve/CN V$_2$) through the infraorbital canal (Wible 2011). The caudal opening of the infraorbital canal, the maxillary foramen, is not well preserved, but it is likely that this canal would run for a short distance through the maxilla based on the infraorbital foramen's proximity to the anteroventral rim of the orbit.

In lateral view, the major feature of the maxilla is the zygomatic process. In DMNH EPV.136181, the zygomatic process has a bifurcated articulation for the associated jugal (see below). The rostroventral rim of the orbit is not perfectly preserved but it is possible that the maxilla may have provided a minor contribution to this region, depending on the extent of the jugal and the lacrimal (Fig. 8). In ventral view, the zygomatic process of the maxilla is visible. The rostral edge of this process begins to form at the level of the paracone of the M1 and thickens laterally to its greatest extent roughly at the level of the metacone of M2. The caudal edge of this process is roughly at the level of the parastyle of M3. Much of the maxilla that would make up
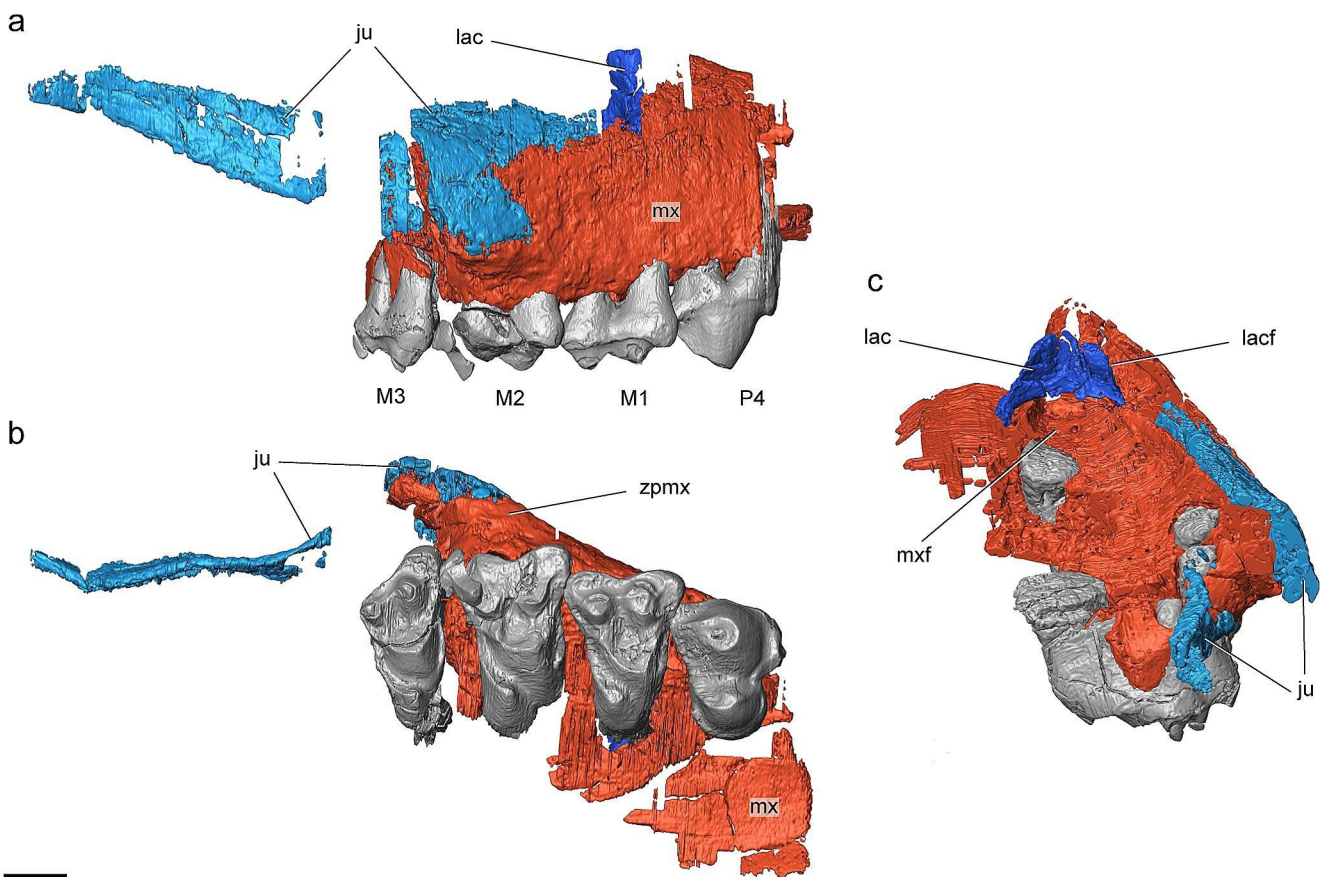
Fig. 8 3D models of the right maxilla, lacrimal, jugal, and preserved upper dentition of *Militocodon lydae* gen. et sp. nov. (DMNH EVP.136181) in lateral (**a**), ventral (**b**), and oblique caudal (**c**) views. Abbreviations: **ju**, jugal; **lac**, lacrimal; **lacf**, lacrimal foramen; **mx**, maxilla; **mxf**, maxillary foramen; **M1**, first upper molar; **M2**; second upper molar; **M3**, third upper molar; **P4**, fourth upper premolar; **zpmx**, zygomatic process of the maxilla. Scale bar equals 2 mm

the hard palate is missing except for some that is medial to the P4, thus the caudal contact with the palatine is not known. In dorsal view, the lingual root of M1, the distobuccal and lingual root of M2 and all three roots of M3 are visibly exposed in the orbital floor.

Jugal. DMNH EPV.136181 partially preserves the right and left jugal, but only the right jugal could be digitally segmented from the μCT data. The right jugal is mostly complete except for some missing portions posterior to the articulation with the maxilla (Fig. 8). The jugal forms most of the zygomatic arch, delimiting the lateral bounds of the temporal fossa, and contacts the maxilla rostrally and the squamosal caudally.

In lateral view, the jugal is dorsoventrally deepest rostrally and progressively shallows caudally. Rostrally, the jugal overlays much of the zygomatic process of the maxilla and then bifurcates into two processes roughly at the level of the caudal root of M2. The shorter ventral process extends rostrally to the level of the caudal root of the M2 whereas the longer dorsal process extends much farther anteriorly, although the rostral extent of this process cannot be determined. Either the long dorsal process of the jugal would contact the lacrimal rostrally, thus excluding the maxilla from the rostroventral orbit, or the jugal would end before contacting the lacrimal, thus giving the maxilla some contribution to the rostroventral orbit.

In dorsal view, the jugal is mediolaterally thin and has an overall gracile appearance. Although this may be partly explained by preservation, it is unlikely that the jugal would be dramatically more mediolaterally wide than what is currently preserved. Caudally, the jugal has a mediolaterally short, flat facet on the dorsal surface for contact with the squamosal. The jugal caudally extends and ends just rostral to the glenoid fossa of the squamosal.

Lacrimal. DMNH EPV.136181 partially preserves the right and left lacrimal bones, although the right is much better preserved (Fig. 8) and will serve as the basis for the following descriptions. The lacrimal is located in the rostral edge of the orbit where this bone typically has contact with several bones including the maxilla, the jugal, the frontal, and sometimes the palatine. Except for the maxilla (and possibly the jugal; see above), most of these contacts are

unclear in DMNH EPV.136181. The orbital process of the lacrimal is extensive and roofs part of the maxillary foramen, the caudal opening of the infraorbital canal. Although the lacrimal foramen is not entirely preserved, an associated groove is preserved on the dorsolateral surface of the lacrimal and the ventromedial surface of the maxilla. This groove represents the nasolacrimal duct and is angled rostrocaudally. The groove terminates posteriorly on the lateral edge within the orbit, indicating that the lacrimal foramen was intraorbital. Although the rostrodorsal portion of the lacrimal is difficult to visualize with μCT data, no lacrimal bone rostrodorsal to the orbit has been identified. Instead, the lacrimal appears to be ventromedial to the maxilla, which suggests DMNH EPV.136181 lacked a facial process of the lacrimal.

Frontal/parietal. DMNH EPV.136181 partially preserves aspects of the frontal and parietal bones, but these are not easily distinguished on the physical specimen or with μCT data and will thus be described together. Running along the midline of the cranium on the dorsal surface is a small sagittal crest (Fig. 7). Rostrally on the endocranial surface, and likely comprised of just the frontal bone, are the large olfactory bulb fossae. This is better preserved on the right side of the specimen. Unfortunately, due to breakage, standard measurements of the olfactory bulbs could not be obtained. Delimiting the olfactory bulb fossae is an annular ridge caudally, separating the olfactory bulbs from the cerebrum of the brain, and a ridge rostrally, which would attach to the cribriform plate of the ethmoid. Rostral to the olfactory bulbs, there is a distinct rounded fossa that is delimited dorsally and ventrally by ridges. This fossa is likely one of several fossae that would have housed ethmoidal turbinates and thus the ridges are likely attachment sites for those turbinates.
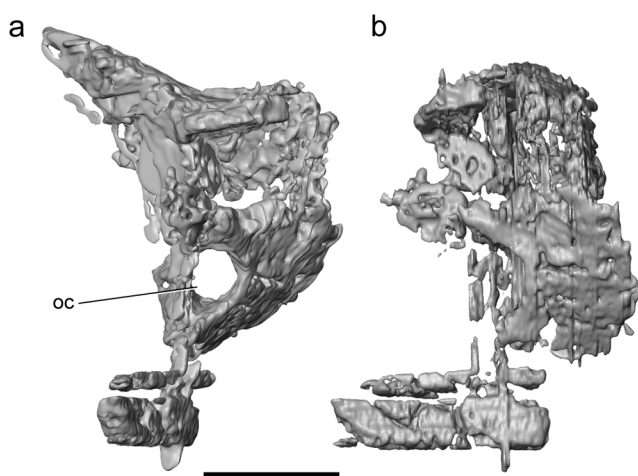

Fig. 9 3D model of the left portion of the orbitosphenoid and presphenoid of *Militocodon lydae* gen. et sp. nov. (DMNH EVP.136181) in anterior (**a**) and lateral (**b**) views. **Abbreviation: oc**, optic canal. Scale bar equals 2 mm

Sphenoid complex. DMNH EPV.136181 partially preserves several bones of the sphenoid complex including the left partial orbitosphenoid and presphenoid and fragments of the right alisphenoid. The left orbitosphenoid is identified as such based on its proximity to the caudal end of the orbit and the presence of a rostrolaterally oriented canal (Fig. 9), which we identify as the optic canal that would transmit the optic nerve (CN II). The optic canal is roughly circular (maximum diameter = 0.85 mm, diameter perpendicular to that = 0.69 mm). The right alisphenoid is less well preserved and only its articulation with the squamosal is preserved. In this articulation, the alisphenoid abutted the entoglenoid process of the squamosal as a small alisphenoid tympanic process on the ventral surface of the cranium.

Squamosal. DMNH EPV.136181 partially preserves the left and right squamosals. Of the left squamosal, part of the zygomatic process is preserved but is little differentiated from the surrounding concretion, while the right squamosal is much better preserved and is better differentiated from the surrounding concretion. Thus, descriptions will be based on the right squamosal (Fig. 10).

In ventral view, the major feature of the squamosal is the glenoid fossa which articulates with the mandibular condyle of the dentary. This fossa is longer mediolaterally than rostrocaudally, matching with the cylindrical condyle exhibited on the dentary. The boundaries of this fossa are not clearly defined and there is only a small lip at the rostral edge of the glenoid fossa. Laterally projecting from the glenoid fossa is the posterior zygomatic root. This posterior zygomatic root projects rostrally to form the zygomatic process of the squamosal which would articulate with the jugal. As described for the jugal, the zygomatic process of the squamosal is mediolaterally narrow and gracile in appearance. Caudal to the glenoid fossa, the postglenoid process is a tall triangular process that does not extend to the full mediolateral width of the fossa. Medial to the postglenoid process, there is a small gap between the postglenoid and what is likely the entoglenoid process. This small gap likely represents the Glaserian fissure that transmits the chorda tympani, a branch of the facial nerve (CN VII) (Wible 2011). Medial to the Glaserian fissure, the squamosal curves ventrally to form part of the entoglenoid process. Caudomedial to the postglenoid process is a large postglenoid foramen (maximum diameter = 1.29 mm), which would transmit the postglenoid vein.

In lateral view, the zygomatic process of the squamosal is dorsoventrally deeper caudally than it is rostrally. This mirrors the pattern which was described for the jugal and its articulation with the maxilla. In this view, the glenoid fossa appears shallow without a major trough-like depression. Caudal to the posterior zygomatic root, there is a partial foramen that is confluent with the postglenoid foramen (Fig. 10), which we interpret to be the suprameatal foramen
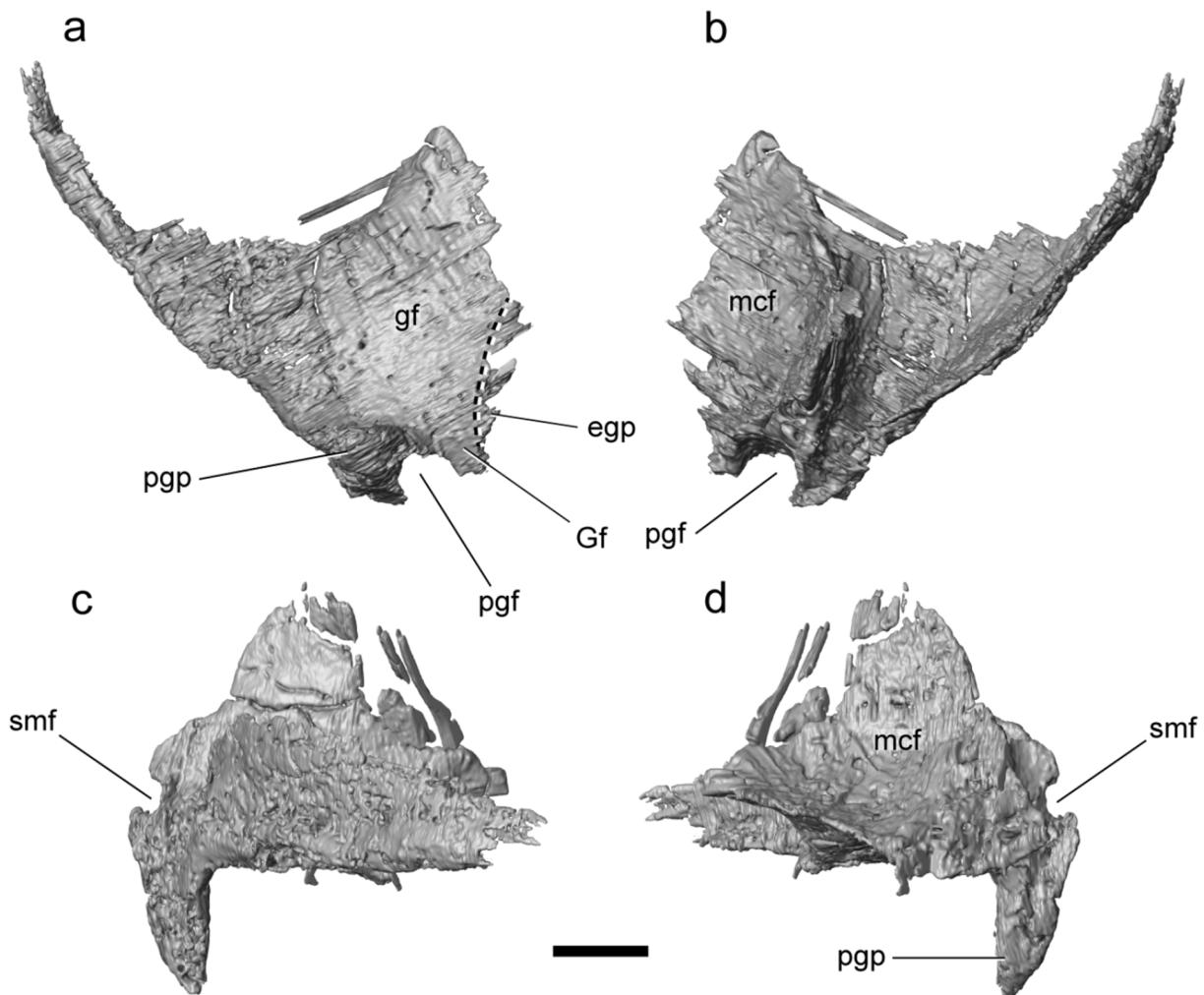
Fig. 10 3D model of the right squamosal of *Militocodon lydae* gen. et sp. nov. (DMNH EVP.136181) in ventral (**a**), dorsal (**b**), lateral (**c**) and medial (**d**) views. Abbreviations: **egp**, entoglenoid process; **Gf**, Glaserian fissure; **gf**, glenoid fossa; **mcf**, middle cranial fossa; **pgf**, postglenoid foramen; **pgp**, postglenoid process; **smf**, suprameatal foramen. Scale bar equals 2 mm

(maximum diameter = 0.75 mm). Dorsal to the glenoid fossa, the squama of the squamosal extends dorsally and forms part of the braincase wall. On the medial aspect, the squama is broadly concave and seemingly has a significant exposure in the middle cranial fossa, although the absence of the parietal in this region prevents from understanding the true extent of this exposure.

Petrosal. DMNH EPV.136181 partially preserves the right and left petrosals. The left petrosal is more complete and preserves aspects of the pars cochlearis and tegmen tympani while the right petrosal preserves the rostral part of the pars cochlearis (Fig. 11).

In DMNH EPV.136181, the partially preserved promontorium is low and somewhat rounded, although the promontorium is incomplete and does not preserve the fenestra

vestibuli or fenestra cochleae and the mastoid region is completely absent. No vascular grooves indicating the route of the internal carotid artery are visible on the surface of the promontorium, although this apparent absence might be from the state of preservation and/or an artifact of digital segmentation of the μCT data. At the rostral edge of the petrosal, there is a rostrally projecting epitympanic wing. This process is straight at its rostral extent with a sub-rectangular appearance. The straight rostral edge of epitympanic wing is dull and appears to lack bony articular facets for the alisphenoid, basisphenoid, or squamosal. This would suggest that DMNH EPV.136181 possessed a patent pyriform fenestra, although it is unclear how large this fenestra would be. DMNH EPV.136181 does not possess a rostral tympanic process of the petrosal. Lateral to the promontorium is the
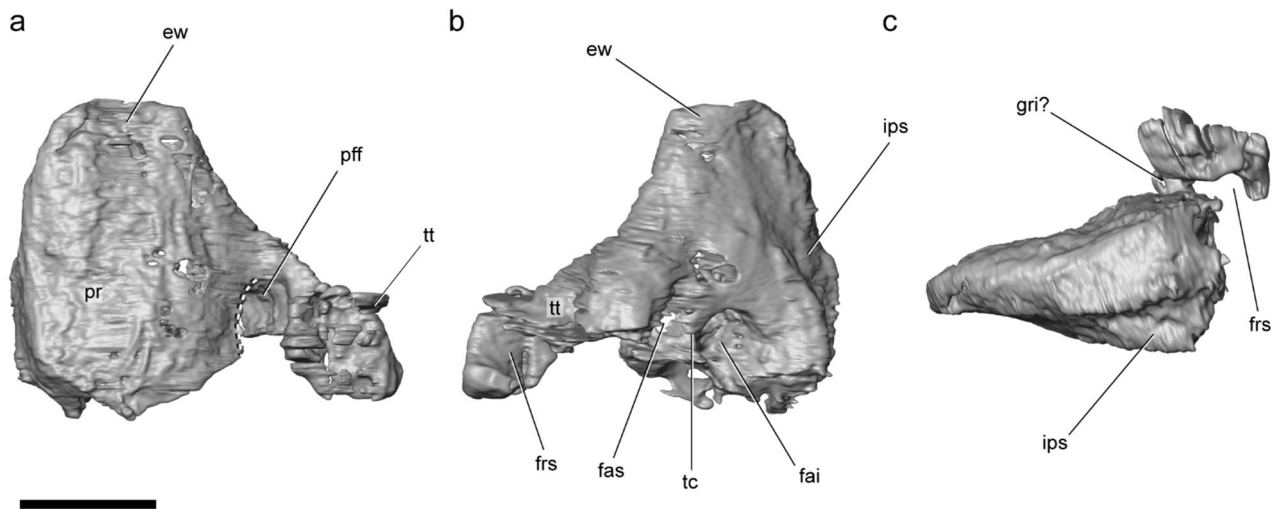
Fig. 11 3D model of the left petrosal of *Militocodon lydae* gen. et sp. nov. (DMNH EVP.136181) in oblique ventral (**a**), oblique dorsal (**b**), and oblique medial (**c**) views. Black dashed line in oblique ventral view illustrates breakage to the floor of the cavum supracochleare. Abbreviations: **ew**, epitympanic wing; **fai**, foramen acousticum infer-ius; **fas**, foramen acousticum superius; **fi**, fossa incudis; **frs**, foramen for ramus superior of the stapedial artery; **gri**, groove for ramus infe-rior of the stapedial artery; **ips**, inferior petrosal sinus; **pff**, primary facial foramen; **pr**, promontorium; **tc**, transverse crest; **tt**, tegmen tym-pani. Scale bar equals 2 mm

partially preserved tegmen tympani, which is a narrow, uninflated ridge with a slight ventral projection. The rostral extent of the tegmen tympani is just rostral to the primary facial foramen. Posteriorly, the tegmen tympani has a par-tially preserved foramen (see below) but is not preserved posterior to this.

There is a partially preserved foramen lateral to the promontorium that likely represents the primary facial fora-men that would transmit the facial nerve (CN VII). In most eutherian mammals, this foramen is not visible in ventral view and is covered by a sheet of bone (Wible 2023). This sheet of bone floors a space called the cavum supracochle-are and creates the secondary facial foramen along the cau-dal margin. In the cavum supracochleare, the facial nerve bulges into the geniculate ganglion and derives two nerves: the rostral greater petrosal nerve and the caudal continua-tion of the facial nerve which would then exit the secondary facial foramen. Only a faint ridge on the tegmen tympani ventral to the primary facial foramen is preserved, which we interpret to be a remnant of the floor to the cavum supra-cochleare. Thus, the secondary facial foramen would likely be present, but is not preserved in DMNH EPV.136181 due to damage. The greater petrosal nerve exits through an opening called the hiatus Fallopii. The hiatus Fallopii is not preserved due to breakage in DMNH EPV.136181, but was likely located just rostral to the primary facial foramen based on our interpretation of the bone which floored of the cavum supracochleare. Thus, the greater petrosal nerve likely exited the hiatus Fallopii at the rostral edge of the tegmen tympani.

In medial view, the groove for the inferior petrosal sinus is visible on the pars cochlearis. This sinus is oriented ros-trocaudally and bounded medially and laterally by distinct ridges. This sinus would connect rostrally with the cavernous sinus on the basisphenoid and with the jugular foramen cau-dally. Unfortunately, due to breakage, DMNH EPV.136181 does not preserve the caudal extent of this sinus and thus the position of the jugular foramen is not preserved. Ventral to the inferior petrosal sinus is a distinctly flat section of the pars cochlearis and may represent an articular facet for the adjacent basioccipital. A large groove oriented rostro-laterally crosses the tegmen tympani (Fig. 11) (maximum diameter = 1.02 mm). We interpret this as the remnant of the foramen for the ramus superior of the stapedial artery, although it is possible that this feature might be confused with and actually represents the tympanic aperture of the prootic canal (MacPhee et al. 2021). This artery is a branch of the stapedial artery that arises after the stapedial artery passes through the obturator foramen of the stapes. After passing through this foramen, the ramus superior would divide into a posterior branch that would supply temporal rami and an anterior branch that would continue anteriorly to occupy the orbitotemporal canal for blood supply to the orbit (Wible 2011). Rostral to this foramen is a smaller groove (maximum diameter = 0.37 mm) oriented rostrocau-dally that may have housed the ramus inferior of the stape-dial artery. Rostrally, the route of this vessel is not preserved due to breakage.

In dorsal view, the major feature is the shallow inter-nal acoustic meatus, which consists of two foramina: the

foramen acusticum superius, which transmits the facial nerve (CN VII) and the vestibular portion of CN VIII, and foramen acusticum inferius, which transmits the rest of CN VIII to innervate the cochlea. These foramina are separated by the crista transversus which is slightly recessed into the internal acoustic meatus.

Comparisons

To best contextualize the morphology of DMNH EPV.136181, we made comparisons to the skull anatomy of other documented periptychids and arctocyonids. Dentary comparisons were made to the following taxa: the large-bodied periptychid *Periptychus carinidens* (AMNH 16995; Shelley et al. 2018); the large-bodied periptychid *Ectoconus ditrigonus* (AMNH 16495; Matthew 1937); the periptychid *Miniconus jeanninae* (UCM 103181; Atteberry and Eberle 2021); the periptychid *Conacodon entoconus* (AMNH 16425; Matthew 1937); the periptychid *Conacodon cophater* (AMNH 16481; Matthew 1937); the periptychid *Conacodon hettingeri* (UCM 103374; Atteberry and Eberle 2021); the periptychid *Ampliconus antoni* (UCM 103150; Atteberry and Eberle 2021); the periptychid(?) *Maiorana noctiluca* (UCM 103147; Atteberry and Eberle 2021); the periptychid(?) *Mimatuta minuial* (YPM-PU 14172); the arctocyonid *Protungulatum gorgun* (UCMP 134558; Lofgren 1995); and the arctocyonid *Sigynorum magnadivisus* (UCM 103133; McComas and Eberle 2016). Cranial comparisons were made to published descriptions of the following large-bodied periptychid taxa: *Periptychus carinidens* (NMMNH P-19482; AMNH 3669; Shelley et al. 2018); *Carsioptychus coarctatus* (AMNH 27601; Matthew 1937); *Ectoconus ditrigonus* (AMNH 16500; Matthew 1937) and smaller bodied periptychids: *Haploconus angustus* (AMNH 3425; Matthew 1937); *Oxyacodon priscilla* (UW 26419; Eberle and Lillegraven 1998); *Conacodon entoconus* (AMNH 3467; Matthew 1937); *Mithrandir gillianus* (AMNH 3601; Matthew 1937); and *Hemithlaeus kowalevskianus* (AMNH 3576; Matthew 1937). Direct comparisons were made to µCT scans of the arctocyonids *Loxolophus hyattianus* (AMNH 16343; Matthew 1937), the large-bodied *Arctocyon primaevus* (MNHN.F. 700, Russell 1960; UCMP 61454), and *Baioconodon denverensis* (DMNH 2500). Additional comparisons were made to the published descriptions of a petrosal attributed to the arctocyonid cf. *Protungulatum* sp. (AMNH 118359; O'Leary 2010).

Dentary. Overall, the dentaries of DMNH EPV.136181 are distinct from those of other more dentally derived periptychids and more similar to those of inferred basal periptychids (e.g., *Maiorana* and *Mimatuta*) and arctocyonids. Differing from that of DMNH EPV.136181, other more

derived periptychids, such as *P. carinidens* (Shelley et al. 2018), *E. ditrigonus* (Matthew 1937), *A. antoni* (Atteberry and Eberle 2021), *Miniconus jeanninae* (Atteberry and Eberle 2021), *C. hettingeri* (Atteberry and Eberle 2021), *C. entoconus* (Matthew 1937), and *C. cophater* (Matthew 1937) have relatively dorsoventrally deeper dentaries. The gracile and relatively dorsoventrally shallower dentary of DMNH EPV.136181 is more similar to the condition exhibited by putatively basal periptychids (e.g., *Mimatuta minuial* and *Maiorana noctiluca*) and arctocyonids (Lofgren 1995; McComas and Eberle 2016). However, similarities among those taxa may be related to their relatively smaller body sizes (e.g., Meloro et al. 2008; Prevosti et al. 2012). All taxa considered here share with DMNH EPV.136181 a mental foramen ventral to the p3, except *Miniconus jeanninae* (Atteberry and Eberle 2021), which has a mental foramen ventral to the caudal root of p2. Although it is unknown if DMNH EPV.136181 had additional mental foramina rostral to the preserved one, two mental foramina are present in *P. carinidens* (Shelley et al. 2018) and *Maiorana noctiluca* (Atteberry and Eberle 2021) with the rostral foramen ventral to p1 in both taxa.

Like that of the inferred basal periptychids, *Mimatuta minuial* and *Maiorana noctiluca*, and arctocyonid taxa, DMNH EPV.136181 likely had a gracile caudoventrally-directed, hook-like angular process. This condition is dramatically different from that of all other known periptychid dentaries, which exhibit an expansion of this region into a large, semicircular process (Matthew 1937; Shelley et al. 2018; Atteberry and Eberle 2021). The rostrocaudal length of the coronoid process relative to its height of DMNH EPV.136181 is similar in proportions to that of other periptychid taxa (Matthew 1937; Shelley et al. 2018; Atteberry and Eberle 2021). The condylar process is positioned relatively high above the alveolar line and is vertically oriented with little to no caudal projection, therefore resembling that of most other periptychids (Matthew 1937; Shelley et al. 2018; Atteberry and Eberle 2021) but differing from that of the inferred basal periptychid *Maiorana noctiluca* (Atteberry and Eberle 2021) and the arctocyonid *Arctocyon primaevus*, which have a condylar process that is lower on the dentary and is much more caudally projecting.

Maxilla. The maxilla of DMNH EVP.136181 is similar to that of other archaic ungulates. For instance, DMNH EVP.136181 shares the position of the infraorbital foramen that is dorsal to the P3 (Fig. 7) with the arctocyonids *L. hyattianus, A. primaevus*, and *B. denverensis*, and the periptychids *P. carinidens* (Shelley et al. 2018) and *E. ditrigonus* (Matthew 1937: plate 24: fig. 1). Differing greatly from that of large-bodied periptychids and from that of some smaller bodied periptychids (e.g., *Haploconus angustus, Mithrandir gillianus, Hemithlaeus*

kowalevskianus), DMNH EVP.136181 lacks a robustly built anterior zygomatic root. In DMNH EVP.136181, the anterior zygomatic root is roughly the length of the M2 and is similar to that of the periptychid *O. priscilla* (Eberle and Lillegraven 1998) and that of the arctocyonid *B. denverensis*. In *C. entoconus* (Matthew 1937: plate 33: fig. 1), the anterior zygomatic root arises at the distal border of P4 and terminates at the distal border of M2. In other periptychids like *P. carinidens* (Shelley et al. 2018: fig. 3), *E. ditrigonus* (Matthew 1937: plate 24: fig. 1), *Haploconus angustus* (Matthew 1937: plate 38: fig. 4), *Hemithlaeus kowalevskianus* (Matthew 1937: plate 35: fig. 1), *Mithrandir gillianus* (Matthew 1937: plate 36: fig. 1b) the anterior zygomatic root begins at the mesial border of the P4 and continues to the distal border of the M2. This condition exhibited by these periptychids is similar to that of the arctocyonid *A. primaevus* where the anterior zygomatic root is more robust and spans the length of several tooth positions.

Jugal. The jugal of DMNH EPV.136181 is gracile and restricted in its contribution to the lateral anterior zygomatic root (Fig. 8) and is in this way more similar to that of the arctocyonids *A. primaevus* (UCMP 61454), *L. hyattianus* (AMNH 16343), and *B. denverensis* (DMNH 2500). This condition differs from that of the periptychid *P. carinidens*, which has a robustly constructed jugal that occupies much of the lateral anterior zygomatic root (Shelley et al. 2018: fig. 3). Both periptychids, including DMNH EPV.136181, and arctocyonids have a rostral bifurcation of the jugal into rostrodorsal and rostroventral processes. However, in DMNH EPV. 136181, the rostroventral process is positioned on the lateral surface of the anterior zygomatic root, which is similar to that of the arctocyonids *A. primaevus*, *L. hyattianus*, and *B. denverensis*, and differs from the periptychids *P. carinidens*, in which the rostroventral process is restricted to the ventral surface of the anterior zygomatic root (Shelley et al. 2018).

Lacrimal. Although the lacrimal is incomplete in DMNH EPV.136181 and not well documented in other archaic ungulates, some comparisons are possible. DMNH EPV.136181 likely lacks a facial process of the lacrimal (Figs. 7 and 8), which is like that of other periptychids (e.g., *Haploconus angustus*, *P. carinidens*, *C. coarctatus*, *E. ditrigonus*; Matthew 1937, Shelley et al. 2018). In this way, DMNH EPV.136181 is different from that of the arctocyonids *A. primaevus* and *B. denverensis*, which have a small triangular facial process of the lacrimal.

Frontal/parietal. Comparisons of this region are limited because the frontal/parietal of DMNH EPV.136181 is not well differentiated and is rather fragmentary. However, based on what is preserved, DMNH EPV.136181

might differ from that described for periptychids and arctocyonids that have large sagittal crests along the midline of the dorsal surface of the cranium. Although, these taxa primarily have their sagittal crests on the paired parietals, which are not well-preserved in DMNH EPV.136181. Primarily differing from these taxa is the absence of a large sagittal crest on the dorsal surface of the cranium along the midline. In DMNH EPV.136181 there is only a faint hint of a sagittal crest, whereas the documented periptychids and arctocyonids all have large, well-developed sagittal crests. However, it should be noted that DMNH EPV.136181 is much smaller than the taxa available for comparison and this difference is likely due at least in part to a relative size difference (e.g., Meloro et al. 2008; Prevosti et al. 2012).

Squamosal. The squamosal of DMNH EPV.136181 is generally similar to that of other archaic ungulates. For instance, like the periptychids *P. carinidens* and *C. coarctatus* (Shelley et al. 2018), and the arctocyonids *A. primaevus*, *B. denverensis, L. hyattianus*, DMNH EPV.136181 has a suprameatal foramen (Fig. 10), which is widely distributed among eutherian clades (Wible et al. 2009; O'Leary et al. 2013). Further sharing similarities among many of the taxa examined here, the glenoid fossa of DMNH EPV.136181 is mediolaterally broader than it is rostrocaudally deep and relatively flat. The arctocyonid *A. primaevus* differs from all other examined taxa, including that of DMNH EPV.136181, in possessing a more cylindrically concave glenoid fossa with a distinct rostral lip-like preglenoid process. The postglenoid process of DMNH EPV.136181 is similar to that described for *P. carinidens* in that both are relatively mediolaterally narrow with little to no rostral inclination (Shelley et al. 2018). This condition differs significantly from that of *A. primaevus*, which has a relatively large postglenoid process that stretches the mediolateral breadth of the glenoid fossa and has a rostral inclination. The condition exhibited by *L. hyattianus* appears to be more similar to that of *A. primaevus* with some rostral inclination, but the postglenoid process does not form the entire posterior wall of the glenoid fossa. All examined taxa have a postglenoid foramen that is caudomedial to the postglenoid process. In DMNH EPV.136181, this foramen is relatively large (Fig. 10) like the condition exhibited by *B. denverensis* and *L. hyattianus*, but differs from the relatively smaller foramen in *P. carinidens*, *C. coarctatus*, *E. ditrigonus*, and *A. primaevus* (Shelley et al. 2018).

The relatively gracile and mediolaterally narrow caudal root of the zygomatic of DMNH EPV.136181 differs from the robust and mediolaterally wide caudal zygomatic root of other periptychids (Matthew 1937; Shelley et al. 2018). *A. primaevus* is similar to DMNH EPV.136181 in having a

mediolaterally narrow caudal zygomatic root. This region is not completely preserved in *L. hyattianus*, but it also appears to be mediolaterally narrow like that of DMNH EPV.136181.

Sphenoid complex. Detailed comparisons of the sphenoid complex are limited due to the fragmentary nature of the specimen.

Petrosal. Detailed comparisons of the petrosal are limited due to the fragmentary nature of the specimen. In comparison to other periptychids for which petrosal anatomy is documented, DMNH EPV.136181 differs in several ways and is more similar to arctocyonid taxa. DMNH EPV.136181 has a rostrally projecting epitympanic wing (Fig. 11), which is unlike that of the periptychid *P. carinidens* (Shelley et al. 2018: fig. 8) and the arctocyonid cf. *Protungulatum* sp. (O'Leary 2010: fig. 3) that only possess some rostral growth from the rostral pole of the promontorium. A cranium with intact petrosals of the periptychid *C. coarctatus* is known (Matthew 1937) and previous work has described the inner ear anatomy and endocast of this specimen (Cameron et al. 2019), but thorough description of the petrosal anatomy is currently lacking. Although a cranium of *E. ditrigonus* has been described (Matthew 1937), its petrosal anatomy was not documented. DMNH EPV.136181 lacks a rostral tympanic process, which is similar to the arctocyonids cf. *Protungulatum* sp. (O'Leary 2010: fig. 3) and *A. primaevus* (UCMP 61454) but differs from the periptychid *P. carinidens* which exhibits this process, albeit it was only tentatively identified and is not well developed (Shelley et al. 2018).

In DMNH EPV.136181, the hiatus Fallopii likely opens at the rostral edge of the tegmen tympani, which would be similar to that of the petrosal attributed to the arctocyonid cf. *Protungulatum* sp. (O'Leary 2010: fig. 3) and the arctocyonid *A. primaevus* (UCMP 61454). DMNH EPV.136181 has a lateral position for the foramen of the ramus superior of the stapedial artery within the tegmen tympani. This condition is similar to that reported for the arctocyonid *A. primaevus* (Shelley et al. 2018) and observed in *L. hyattianus*, but differs from the periptychid *P. carinidens*, which does not have a foramen in the tegmen tympani for the ramus superior of the stapedial artery (Shelley et al. 2018). The position of this foramen is not known for the arctocyonids *B. denverensis* or cf. *Protungulatum* sp. and not reported for the periptychids *C. coarctatus* and *E. ditrigonus*. DMNH EPV.136181 has an inferred bifurcation of the stapedial artery into its inferior and superior branches within the tympanic cavity and is similar to that the periptychid *P. carinidens* (Shelley et al. 2018) and the arctocyonids *B. denverensis*, *A. primaevus*, *L. hyattianus* in this regard, although this pattern is likely primitive for eutherian mammals (Wible 1983).

Discussion

***Militocodon* and periptychid evolutionary relationships.** The dentition of *Militocodon lydae* exhibits all proposed conacodontine synapomorphies (Archibald et al. 1983a, b) yet is distinctly plesiomorphic relative to that *Oxyacodon*; thus, we interpret *Militocodon* as a basal member of the Conacodontinae. Further, our comparisons among periptychids, including the specimens of *Militocodon lydae* described here, raise questions about the monophyly of *Oxyacodon* and phylogenetic relationships near the base of Periptychidae. In a recent study of periptychid phylogenetic relationships (Shelley 2018), *Oxyacodon* spp. were recovered as a paraphyletic grade stemward of *Conacodon* spp. Such an interpretation is consistent with our qualitative observations of different species of *Oxyacodon*. For example, *O. apiculatus* and *O. priscilla*, due primarily to their hypocones having bases that slope less prominently lingually and their lower molars exhibiting prominent postcingulids and longer paracristids, bear a closer resemblance to *Militocodon* than does *O. agapetillus*, which more closely resembles *Conacodon* (sensu Archibald 1982; Archibald et al. 1983b) in exhibiting a shorter talonid and very reduced paraconid positioned at the mesiolingual base of the protoconid. In this way, the dental morphology of *Oxyacodon* spp. adds to a morphocline within the Conacodontinae that bridges the gap between the relatively plesiomorphic *Militocodon* and the relatively apomorphic *Conacodon*. Since the last revision of the genus *Oxyacodon* (Archibald et al. 1983a), numerous new periptychid taxa and specimens have been described; as such, the monophyly of *Oxyacodon* and its relationship among other periptychids requires additional study that is beyond the scope of this paper.

That *Militocodon* bears some resemblance to *Mimatuta* and *Maiorana* suggests that those dental similarities are either (1) periptychid synapomorphies and *Mimatuta* and *Maiorana* represent the basalmost members of the Periptychidae as previously hypothesized (e.g., Van Valen 1978; Archibald et al. 1983b; Archibald 1998); or (2) symplesiomorphies and thus cannot be used to reconstruct evolutionary relationships. Most recent results of phylogenetic analyses have recovered *Mimatuta* and *Maiorana* as nested within (an often monophyletic) Arctocyonidae (McComas and Eberle 2016; Shelley 2018; Atteberry and Eberle 2021). Although the seemingly intermediate dental morphology of *Militocodon* may contribute to resolving questions regarding the phylogenetic position of *Mimatuta* and *Maiorana* and broader interrelationships among periptychids, relevant published character-taxon matrices (e.g., McComas and Eberle 2016; Atteberry and Eberle 2021) were not originally designed to adequately test those hypotheses (as acknowledged by those authors).

The Atteberry and Eberle (2021) matrix (derived from McComas and Eberle 2016) is based solely on primarily qualitative dental characters, which could lead to a less accurate phylogenetic reconstruction (Sansom et al. 2017). This matrix also lacks all species of *Oxyacodon* and more derived periptychids (e.g., *Periptychus* and *Ectoconus*), which are necessary to fully test periptychid phylogenetic hypotheses. Remedying these issues is beyond the scope of this project. As such, future work revising existing dental characters, adding cranial and postcranial characters, and including a more holistic taxonomic sample of Paleocene archaic ungulates is needed to fully test the phylogenetic implications of *Militocodon lydae* within the Periptychidae.

Beyond the current lack of appropriately rigorous character-taxon matrices and possibly key intermediate taxa (e.g., *Militocodon*), the recent recovery of *Mimatuta* and *Maiorana* as arctocyonids may be a result of the typical, bifurcating cladistic models. The observed explosive radiation of archaic ungulates in the early aftermath of the K–Pg mass extinction is unlikely to be adequately captured via bifurcating models that tend to mask rapid evolutionary radiations and obscure probable ancestor-descendent relationships in the fossil record (e.g., Crouch et al. 2021). Allowing for budding in the branching model of future cladistic analyses may reveal that many early periptychid taxa (including *Militocodon*) were descended from *Mimatuta*- or *Maiorana*-like ancestors.

The dentition of *Militocodon* is distinctive in being truly intermediate, straddling the gap between the more basal portions of the periptychid tree and its more deeply nested branches. It highlights the importance of new fossil discoveries and descriptions in understanding evolutionary relationships, simultaneously reinforcing some hypotheses while calling others into question. The continued discovery and study of early Paleocene archaic ungulates will almost certainly reveal more specimens that do not fit neatly into existing taxonomic bins, forcing us to contend with an evolutionary history tangled by evolutionary grades and transitional forms.

**Implications of the skull morphology of *Militocodon*.** Cranial remains of early Paleocene placental mammals are rare and many of the preserved crania represent larger-bodied and/or more derived members within their respective clades. This is especially true of the Periptychidae in which the crania that have been described represent relatively large and derived members such as *Periptychus carinidens, Carsioptychus coarctatus*, and *Ectoconus ditrigonus*. The partial skull described here of *Militocodon lydae*, a small-bodied periptychid (273–455 g; see 'Materials and methods' above) with relatively primitive dentition, thus has the possibility to elucidate primitive cranial morphology of periptychids, which could help detangle interrelationships among early Paleocene archaic ungulates and other placental mammals.

Despite numerous dental synapomorphies of *Militocodon* and other periptychids, to the best of our knowledge, *Militocodon* does not preserve a single cranial synapomorphy with that of other periptychids. In each region of the cranium, *Militocodon* resembles that of the other archaic ungulates (e.g., arctocyonids) or that which has been reconstructed for the primitive placental mammal (e.g., presence of foramen for superior ramus of stapedial artery) (O'Leary et al. 2013). This apparent absence of cranial synapomorphies between *Militocodon* and other periptychids suggests that the cranial morphology of periptychids is not distinct from that of a primitive placental mammal and thus Periptychidae cannot be diagnosed based on cranial morphology alone. Although there are clear cranial similarities among large-bodied periptychid taxa (e.g., developed sagittal crest, robustly built zygomatic arch, greatly expanded angular process of the dentary), they all belong to the subfamily Periptychinae and were supported as closely related in a recent phylogenetic analysis of the Periptychidae (Shelley 2018). Thus, these shared features might be more diagnostic for periptychines and not for the Periptychidae as a whole. Further, many of these shared features are likely subject to positive allometry or are directly related to biomechanical needs of mastication (e.g., Meloro et al. 2008; Prevosti et al. 2012). For instance, the robust zygomatic arch and large angular process that these periptychines exhibit are likely the result of the increased importance the masseter and internal pterygoid has during a grinding or crushing mastication (Radinsky 1985). Thus, the small-bodied *Militocodon* without the dramatic dental adaptations of the periptychines might be expected to lack such features.

Trends in conacodontine dental evolution. Since first erected, the Conacodontinae were envisaged as a morphocline from 'primitive' periptychids like *Mimatuta* to *Oxyacodon* then from *Oxyacodon* to *Conacodon* (Van Valen 1978; Archibald 1982; Archibald et al. 1983a, b). *Militocodon lydae* fits this 'conacodontine morphocline hypothesis'; its molar morphology is intermediate between the putatively basal periptychids *Mimatuta* and *Maiorana* and *Oxyacodon* (Fig. 12). Along this morphocline leading from *Mimatuta*/*Maiorana* to *Conacodon* we see the following trends in the upper molars: (1) the hypocone: (i) increases in size, (ii) shifts mesiolingual to a position at or near the mesiodistal midline of the tooth, and (iii) lingual base projects farther lingually to form a long shallow slope to its apex; (2) the para- and metastylar lobes decrease in width and the ectoflexus becomes shallow; (3) the protocone shifts farther buccally to become closely appressed to the paracone and metacone, which, in concert with the mesiolingual shift of the hypocone, results in a more triangular occlusal outline;

Fig. 12 Conacodontine morphocline hypothesis, wherein the plesiomorphic periptychid dental character states exhibited by *Mimatuta* and *Maiorana* grade into the apomorphic states exhibited by *Conacodon*. *Militocodon lydae* exhibits a dental morphology that is intermediate between *Mimatuta*/*Maiorana* and *Oxyacodon*. Left M/m2 are shown
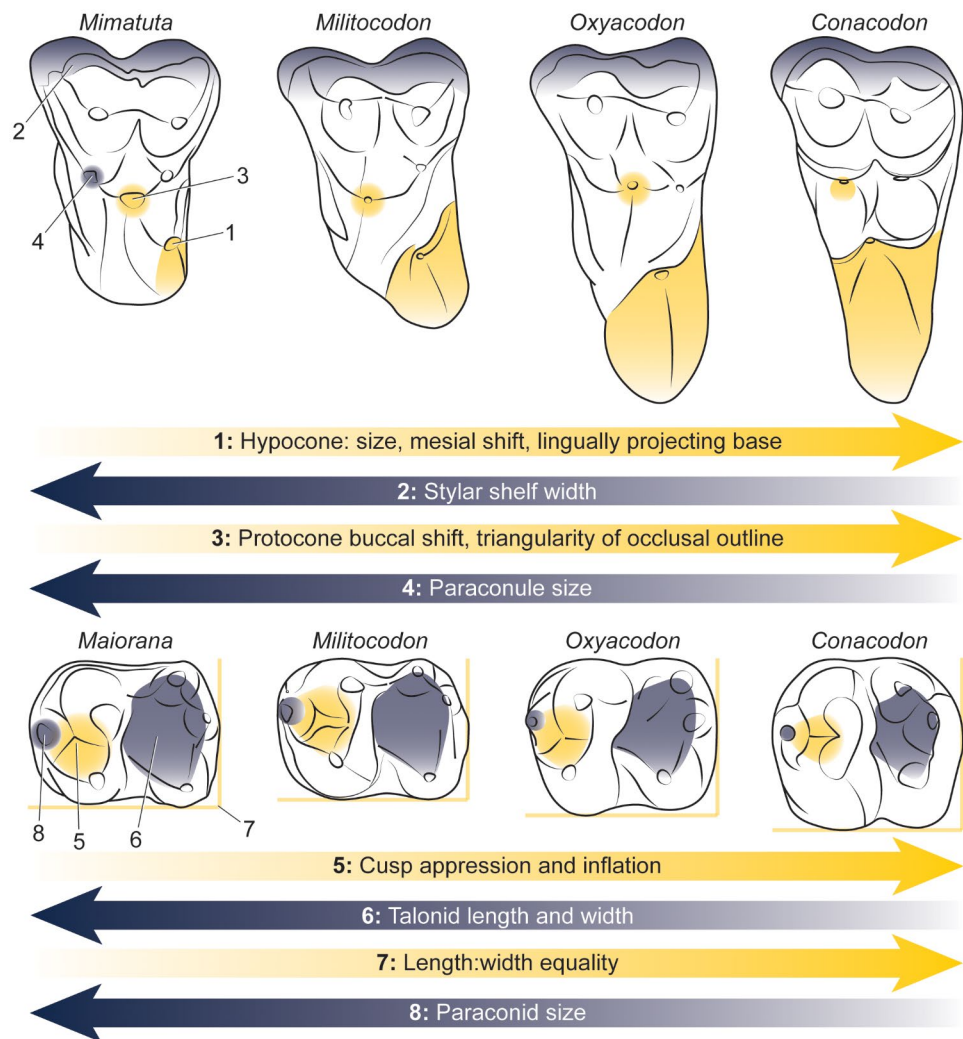
and (4) a reduction and eventual disappearance of the paraconule and an enlargement of the metaconule. Similarly, in the lower molars we see: (1) a greater appression and inflation of the trigonid and talonid cusps; (2) a shortening and narrowing of the talonid basin; (3) increasingly more square length-to-width ratio; and (4) a reduction in paraconid size. That suite of character transformations that epitomize the conacodontine morphocline can be summarized as a greater appression and inflation of the primary molar cusps and a greater dominance of the hypocone in increasingly transverse upper molars (Fig. 12).

It is possible that these trends in conacodontine dental evolution are not adaptively meaningful nor the result of directional selection (e.g., Simpson 1944; Gould and Lewontin 1979); yet the morphocline represented by the cheek teeth of *Mimatuta*/*Maiorana*–*Militocodon*–*Oxyacodon*–*Conacodon* must have been functionally viable (e.g., Szalay 1981; Butler 2000), raising the question as to what masticatory behaviors underlie those striking

dental morphologies. The increasing inflation and appression of the molar cusps, as well as an increase in the size of posterior premolars relative to the molars, are trends observed among all periptychids, not just conacodontines, and these trends apparently reflect a greater specialization for durophagy and orthal-crushing mastication (e.g., Matthew 1937; Simpson 1937b; Archibald 1982; Rensberger 1986). Indeed, the behavioral precursors of crushing food at the level of the posterior premolars may be reflected in the wear patterns observed in the holotype of *Militocodon lydae* (DMNH EPV.136181)—the principal cusps of P/p4 and M/m1 are much more heavily worn than M/m2 and M/m3 (Fig. 4). Although the earlier eruption of M/m1 relative to M/m2–3 likely contributed to that pattern, P/p4 are typically the last premolars to erupt among most eutherian mammals (including ungulates; e.g., Ziegler 1971; Smith 2000; Luo et al. 2004), suggesting that the heavy wear on P/p4 may indeed reflect masticatory behavior, not ontogeny.

Unique to conacodontines, however, is the dramatic increase in the size and mesiolingual projection of the hypocone. The appearance of the hypocone among therian mammals in the Cenozoic has been well documented (e.g., Matthew 1937) and has been hypothesized to be a functional prerequisite to specialized herbivory among therians by increasing the occlusal surface area and essentially 'squaring off' the upper molars (Hunter and Jernvall 1995). Nonetheless, the trend in hypocone enlargement among conacodontines does not follow that pattern; instead, the greater lingual expansion of the hypocone is associated with a distinct mesiolingual shift of its apex, essentially making the molar more triangular and transverse in occlusal outline (Fig. 12). Consequently, the prominence of the conacodontine hypocone does not square off the occlusal surface area of the molars but rather maintains or even makes more pronounced the embrasure between molars moving from *Militocodon* to *Conacodon*.

The function of the hypocone in conacodontines is therefore likely non-analogous to those of other Cenozoic mammals, and it likely did not participate in Phase II grinding, at least not in the same way as geologically younger eutherian mammals (Kay and Hiiemae 1974; Rensberger 1986; Hunter and Fortelius 1994; Janis 1990). Indeed, there is little to no evidence of hypocone-involved Phase II occlusion among Puercan mammals from the Littleton fauna of the Denver Basin, including the lower dentition of *Conacodon harbourae*, the wear patterns on which were interpreted as resulting from primarily Phase 1 occlusal contact with the paracone, metacone, and protocone (Dewar 2003; see also Rensberger 1986). Supporting this interpretation is the observation that the hypocones of conacodontines are only moderately worn if at all, in contrast with the more substantial wear on the paracones, metacones, and protocones (e.g., Archibald et al. 1983a, b). Thus, we hypothesize that the lingual expansion of the hypocone on conacodontines was not an adaptation for increased transverse or proal grinding area but rather for increased orthal shearing and crushing on the lingual aspect of the molars. The grooves between the hypocone and protocone and between the protocone (+ metaconule) and paracone and metacone would fit well into the foreshortened lingual and buccal walls of the talonid basin, tightly occluding to shear and crush food rather than increasing surface area for medially directed grinding. Such a function would also explain the relative lack of wear on the hypocones because the apices of those cusps essentially never made occlusal contact with the lower teeth (e.g., Butler 1972), but rather only contacted food particles along the lingual margin of the lower molar. In sum, the conacodontine morphocline may reflect an increasing prevalence of orthal shearing and crushing mastication, driven by increasingly transverse upper molars and associated intercusp grooves occluding tightly within the buccal and lingual margins of increasingly foreshortened talonids.

Conclusion

The skull of the new periptychid, *Militocodon lydae*, described here simultaneously illuminates and complicates the early evolutionary history of the Periptychidae (and archaic ungulates more broadly). On one hand, the well-preserved and associated dentition of DMNH EPV.136181 reveals consistent trends in conacodontine dental evolution, and suggests rapid exploration of new masticatory niches among archaic ungulates in the early Paleocene. On the other hand, the skull of the small-bodied and relatively phylogenetically basal *Militocodon*, which could have been greatly informative phylogenetically, is frustratingly devoid of diagnostic characters, suggesting that the apomorphies that inform ordinal relationships among Paleocene eutherian mammals may be even more elusive in the cranium than they are in the dentition. Nonetheless, the skull of *Militocodon* is only patchily preserved, and of the few Paleocene-mammal crania that are known, even fewer are described, greatly inhibiting our understanding of phylogenetically informative cranial features. Ultimately, the obscurity of periptychid interrelationships is likely the product of their rapid diversification after the K–Pg boundary; taxa near the base of rapid evolutionary radiations are often very difficult to distinguish from one another morphologically due to the rapidity of their divergence and the absence of accumulated phenotypic differences (e.g., Simpson 1944; Gingerich 2019; Goswami et al. 2022). The discovery and thorough description of more complete periptychid and other archaic ungulate fossils from the Puercan, like the holotype of *Militocodon lydae* described here, are necessary to better illuminate the complex evolutionary history of this important group of Paleocene mammals.

Author contributions LNW, JWC, SGBC, and TRL conceived of the project, LNW and JWC wrote the first draft of the manuscript, conducted the analyses, and prepared the figures with substantial contributions from SGBC and TRL. LNW and JWC are co-corresponding and co-first authors.

Declarations

References

Alroy J (1999) The fossil record of North American mammals: evidence for a Paleocene evolutionary radiation. Syst Biol 48:107–118.

Archibald JD (1982) A study of Mammalia and geology across the Cretaceous-Tertiary boundary in Garfield County, Montana. Univ Calif Publ Geol Sci 122:1–286.

Archibald JD (1993) The importance of phylogenetic analysis for the assessment of species turnover: a case history of Paleocene mammals from North America. Paleobiology 19:1–27.

Archibald JD (1998) Archaic ungulates ('Condylarthra'). In: Janis CM, Scott KM, Jacobs LL (eds) Evolution of Tertiary Mammals of North America, Volume 1: Terrestrial Carnivores, Ungulates, and Ungulate like Mammals. Cambridge University Press, pp 292–329.

Archibald JD, Rigby Jr JK, Robison SF (1983a) Systematic revision of *Oxyacodon* (Condylarthra, Periptychidae) and a description of *O. ferronensis* n. sp. J Paleontol 57:53–72.

Archibald JD, Schoch RM, Rigby Jr JK (1983b) A new subfamily, Conacodontinae, and new species, *Conacodon kohlbergeri*, of the Periptychidae (Condylarthra, Mammalia). Postilla 191:1–24.

Archibald JD, Zhang Y, Harper T, Cifelli RL (2011) *Protungulatum*, confirmed Cretaceous occurrence of an otherwise Paleocene eutherian (placental?) mammal. J Mammal Evol 18:153–161.

Atteberry MR, Eberle JJ (2021) New earliest Paleocene (Puercan) periptychid 'condylarths' from the Great Divide Basin, Wyoming, USA. J Syst Palaeontol 19:565–593.

Barclay RS, Johnson KR, Betterton WJ, Dilcher DL (2003) Stratigraphy and megaflora of a KT boundary section in the eastern Denver Basin, Colorado. Rocky Mt Geol 38:45–71.

Bown TM, Kraus MJ (1979) Origin of the tribosphenic molar and metatherian and eutherian dental formulae. In: Lillegraven JA, Kielan-Jaworowska Z, Clemens WA (eds) Mesozoic Mammals: the First Two-Thirds of Mammalian History. University of California Press, Berkeley, pp 172–181.

Brown RW (1943) Cretaceous-Tertiary boundary in the Denver Basin, Colorado. Bull Geol Soc Am 54:65–86.

Butler PM (1972) Some functional aspects of molar evolution. Evolution 26:474–483.

Butler PM (2000) Review of the early allotherian mammals. Acta Palaeontol Pol 45:317–342.

Cameron J, Shelley SL, Williamson TE, Brusatte SL (2019) The brain and inner ear of the early Paleocene "condylarth" *Carsioptychus coarctatus*: implications for early placental mammal neurosensory biology and behavior. Anat Rec 302:306–324.

Claytor JR, Weaver LN, Tobin TS, Wilson Mantilla GP (2022) New mammalian local faunas from the first ca. 80 ka of the Paleocene in northeastern Montana and a revised model of biotic recovery from the Cretaceous-Paleogene mass extinction. J Vertebr Paleontol 42:e2222777.

Clemens WA (2002) Evolution of the mammalian fauna across the Cretaceous-Tertiary boundary in northeastern Montana and other areas across the Western Interior. In: Hartman JH, Johnson KR, Nichols DJ (eds) The Hell Creek Formation and the Cretaceous–Tertiary Boundary in the Northern Great Plains: an Integrated Continental Record of the End of the Cretaceous. Geol Soc Am Spec Pap 361, Boulder, pp 217–245.

Cope ED (1882) A new type of Perissodactyla. Am Nat 15:1017–1018.

Crouch NM, Edie SM, Collins KS, Bieler R, Jablonski D (2021) Calibrating phylogenies assuming bifurcation or budding alters inferred macroevolutionary dynamics in a densely sampled phylogeny of bivalve families. Proc R Soc B 288:20212178.

Dewar EW (2003) Functional diversity within the Littleton fauna (early Paleocene), Colorado: evidence from body mass, tooth structure, and tooth wear. PaleoBios 23:1–19.

Eberle JJ (2003) Puercan mammalian systematics and biostratigraphy in the Denver Formation, Denver Basin, Colorado. Rocky Mt Geol 38:143–169.

Eberle JJ, Lillegraven JA (1998) A new important record of earliest Cenozoic mammalian history: Eutheria and paleogeographic / biostratigraphic summaries. Rocky Mt Geol 33:49–117.

Flynn AG, Davis AJ, Williamson TE, Heizler M, Fenley CW, Leslie CE, Secord R, Brusatte SL, Peppe DJ (2020) Early Paleocene magnetostratigraphy and revised biostratigraphy of the Ojo Alamo Sandstone and lower Nacimiento formation, San Juan Basin, New Mexico, USA. Geol Soc Am Bull 132:2154–2174.

Fuentes AJ, Clyde WC, Weissenburger K, Bercovici A, Lyson TR, Miller IM, Ramezani J, Isakson V, Schmitz MD, Johnson KR (2019) Constructing a time scale of biotic recovery across the Cretaceous–Paleogene boundary, Corral Bluffs, Denver Basin, Colorado, USA. Rocky Mt Geol 54:133–153.

Gill T (1872) Arrangements of the families of mammals: with analytical tables. Smithson Misc Collect 6:1–98.

Gingerich PD (2019) Rates of Evolution: a Quantitative Synthesis. Cambridge University Press, Cambridge, UK.

Goswami A, Noirault E, Coombs EJ, Clavel J, Fabre AC, Halliday TJ, Churchill M, Curtis A, Watanabe A, Simmons NB, Beatty BL (2022) Attenuated evolution of mammals through the Cenozoic. Science 378:377–383.

Gould SJ, Lewontin RC (1979) The spandrels of San Marco and the Panglossian paradigm: a critique of the adaptationist programme. Proc R Soc Lond B 205:581–598.

Gradstein FM, Ogg JG, Schmitz M, Ogg G (2012) The Geologic Time Scale 2012. Elsevier, Amsterdam, Netherlands.

Hicks JF, Johnson KR, Obradovich JD, Miggins DP, Tauxe L (2003) Magnetostratigraphy of Upper Cretaceous (Maastrichtian) to lower Eocene strata of the Denver Basin, Colorado. Rocky Mt Geol 38:1–27.

Hunter JP, Fortelius M (1994) Comparative dental occlusal morphology, facet development, and microwear in two sympatric species of *Listriodon* (Mammalia: Suidae) from the middle Miocene of Western Anatolia (Turkey). J Vertebr Paleontol 14:105–126.

Hunter JP, Jernvall J (1995) The hypocone as a key innovation in mammalian evolution. Proc Natl Acad Sci USA 92:10718–10722.

Janis CM (1990) The correlation between diet and dental wear in herbivorous mammals, and its relationship to the determination of diets of extinct species. In: Boucot AJ (ed) Evolutionary Paleobiology of Behavior and Coevolution. Elsevier Science Publishers, New York, pp 241–259.

Johnston PA, Fox RC (1984) Paleocene and Late Cretaceous mammals from Saskatchewan, Canada. Palaeontogr Abt A: Palaeozool – Stratigr 186:163–222.

Kay RF, Hiiemae KM (1974) Jaw movement and tooth use in recent and fossil primates. Am J Phys Anthrop 40:227–256.

Kelly TS (2014) Preliminary report on the mammals from Lane's Little Jaw Site Quarry: a latest Cretaceous (earliest Puercan?) local fauna, Hell Creek Formation, southeastern Montana. Paludicola 10:50–91.

Kielan-Jaworowska Z, Cifelli RL, Luo Z-X (2004) Mammals from the Age of Dinosaurs: Origins, Evolution, and Structure. Columbia University Press, New York.

Krause DW, Hoffmann S, Lyson TR, Dougan LG, Petermann H, Tecza A, Chester SGB, Miller IM (2021) New skull material of *Taeniolabis taoensis* (Multituberculata, Taeniolabididae) from the early Paleocene (Danian) of the Denver Basin, Colorado. J Mamm Evol 28:1083–1143.

Legendre, S (1986) Analysis of mammalian communities from the late Eocene and Oligocene of southern France. Palaeovertebrata 16:191–212.

Lillegraven JA, Bieber SL (1986) Repeatability of measurements of small mammalian fossils with an industrial measuring scope. J Vertebr Paleontol 6:96–100.

Linnaeus C (1758) Systema Naturae per Regna Tria Naturae, Secundum Classes, Ordines, Genera, Species, cum Characteribus, Differentiis, Synonymis, Locis. Regnum Animale. Volume 1. 10th Edition. Holmiae (Salvius), Stockholm, Sweden.

Lofgren DL (1995). The Bug Creek problem and the Cretaceous-Tertiary transition at McGuire Creek, Montana. Univ Cal Publ Geol Sci 140: 1–185.

Lofgren DL, Lillegraven JA, Clemens WA, Gingerich PD, Williamson TE (2004) Paleocene biochronology: the Puercan through Clarkforkian land mammal ages. In: Woodburne MO (ed) Late Cretaceous and Cenozoic Mammals of North America: Biostratigraphy and Geochronology. Columbia University Press, New York, pp. 43–105.

Luo Z-X, Kielan-Jaworowska Z, Cifelli RL (2004) Evolution of dental replacement in mammals. Bull Carnegie Mus Nat Hist 36:159–175.

Lyson TR, Miller IM, Bercovici AD, Weissenburger K, Fuentes AJ, Clyde WC, Hagadorn JW, Butrim MJ, Johnson KR, Fleming RF, Barclay RS, Maccracken SA, Lloyd B, Wilson GP, Krause DW, Chester SGB (2019) Exceptional continental record of biotic recovery after the Cretaceous–Paleogene mass extinction. Science 366:977–983.

MacPhee RD, Del Pino SH, Kramarz A, Forasiepi AM, Bond M, Sulser RB (2021) Cranial morphology and phylogenetic relationships of Trigonostylops wortmani, an Eocene South American native ungulate. Bull Am Mus Nat Hist 449:1–83.

Matthew WD (1937) Paleocene faunas of the San Juan Basin, New Mexico. Trans Am Philos Soc 30:1–510.

McComas KM, Eberle JJ (2016) A new earliest Paleocene (Puercan) arctocyonid mammal from the Fort Union Formation, Great Divide Basin, Wyoming, and its phylogenetic position among early 'condylarths.' J Syst Palaeontol 14:445–459.

Meloro C, Raia P, Piras P, Barbera C, O'Higgins PA (2008) The shape of the mandibular corpus in large fissiped carnivores: allometry, function and phylogeny. Zool J Linn Soc 154:832–845.

Middleton MD, Dewar EW (2004) New mammals from the early Paleocene Littleton fauna (Denver Formation, Colorado). Bull N M Mus Nat Hist Sci 26:59–80.

Nessov LA, Archibald JD, Kielan-Jaworowska Z (1998) Ungulate-like mammals from the Late Cretaceous of Uzbekistan and a phylogenetic analysis of Ungulatomorpha. In: Beard KC, Dawson MR (eds) Dawn of the Age of Mammals in Asia. Bull Carnegie Mus Nat Hist 34, Pittsburgh, pp 40–88.

Nichols DJ, Fleming, RF (2002) Palynology and palynostratigraphy of Maastrichtian, Paleocene, and Eocene strata in the Denver Basin, Colorado. Rocky Mt Geol 37:135–163.

O'Leary MA (2010) An anatomical and phylogenetic study of the osteology of the petrosal of extant and extinct artiodactylans (Mammalia) and relatives. Bull Am Mus Nat Hist 335:1–206.

O'Leary MA, Bloch JI, Flynn JJ, Gaudin TJ, Giallombardo A, Giannini NP, … Cirranello AL (2013) The placental mammal ancestor and the post–K-Pg radiation of placentals. Science 339:662–667.

Prevosti FJ, Turazzini GF, Ercoli MD, Hingst-Zaher E (2012) Mandible shape in marsupial and placental carnivorous mammals: a morphological comparative study using geometric morphometrics. Zool J Linn Soc 164:836–855.

Radinsky L (1985). Patterns in the evolution of ungulate jaw shape. Am Zool 25:303–314.

Raynolds RG (1997) Synorogenic and postorogenic strata in the central Front Range, Colorado. In: Boyland BD, Sonnenberg SS (eds) Geologic History of the Colorado Front Range, Rocky Mt Assoc Geologists, pp 43–47.

Raynolds RG (2002) Upper Cretaceous and Tertiary stratigraphy of the Denver Basin, Colorado. Rocky Mt Geol 37:111–134.

Rensberger JM (1986) Early chewing mechanisms in mammalian herbivores. Paleobiology 12:474–494.

Rogers RR, Brady ME (2010) Origins of microfossil bonebeds: insights from the Upper Cretaceous Judith River Formation of north-central Montana. Paleobiology 36:80–112.

Russell DE (1960) L'anatomie cranienne de deux Créodontes du Paléocène de France. Bull Soc Geol France 7:195–199.

Sansom, R. S., Wills, M. A., & Williams, T. (2017). Dental data perform relatively poorly in reconstructing mammal phylogenies: morphological partitions evaluated with molecular benchmarks. Syst Biol 66:813–822.

Shelley SL (2018) The rise of placental mammals: the anatomy, palaeobiology and phylogeny of *Periptychus* and the Periptychidae. Dissertation, University of Edinburgh.

Shelley SL, Williamson TE, Brusatte SL (2018) The osteology of *Periptychus carinidens*: a robust, ungulate-like placental mammal (Mammalia: Periptychidae) from the Paleocene of North America. PLoS ONE 13:e0200132.

Silviria JS (2019) Eutherian biogeography during the Puercan North American Land Mammal age (Paleocene, earliest Danian): problems and potential solutions. Master's Thesis, University of New Mexico.

Simpson GG (1937a) The beginning of the age mammals. Biol Rev Camb Philos Soc 12:1–46.

Simpson GG (1937b) The Fort Union of the Crazy Mountain field, Montana, and its mammalian faunas. Bull U S Natl Mus 169:1–287.

Simpson GG (1944) Tempo and Mode in Evolution. Columbia University Press, New York.

Smith BH (2000) 'Schultz's rule' and the evolution of tooth emergence and replacement patterns in primates and ungulates. In: Teaford MF, Smith MM, and Ferguson MWJ (eds) Development, Function and Evolution of Teeth. Cambridge University Press, pp 212–227.

Smith SM, Sprain CJ, Clemens WA, Lofgren DL, Renne PR, Wilson GP (2018) Early mammalian recovery after the end-Cretaceous mass extinction: a high-resolution view from McGuire Creek area, Montana, USA. Geol Soc Am Bull 130:1–15.

Sprain CJ, Renne PR, Clemens WA, Wilson GP (2018) Calibration of chron C29r: New high-precision geochronologic and

paleomagnetic constraints from the Hell Creek region, Montana. Geol Soc Am Bull 130:1615–1644.

Szalay FS (1981) Functional analysis and the practice of phylogenetic methods as reflected by some mammalian studies. Am Zool 21:37–45.

Van Valen L (1978) The beginning of the age of mammals. Evol Theory 4:45–80.

Wible JR (1983). The internal carotid artery in early eutherians. Acta Palaeontol Pol 28:281–293.

Wible JR (2011) On the treeshrew skull (Mammalia, Placentalia, Scandentia). Ann Carnegie Mus 79:149–230.

Wible JR (2023). The ear region of the Philippine flying lemur *Cynocephalus volans* (Placentalia, Dermoptera). Anat Rec 306:2853–2871.

Wible JR, Rougier GW, Novacek MJ, Asher RJ (2009) The eutherian mammal *Maelestes gobiensis* from the Late Cretaceous of Mongolia and the phylogeny of Cretaceous Eutheria. Bull Am Mus Nat Hist 327:1–123.

Williamson TE, Carr TD (2007) Revision of the problematic early Paleocene genus *Oxyclaenus* (Mammalia: Oxyclaenidae) and a new species of *Carcinodon*. J Vertebr Paleontol 27:973–986.

Williamson TE, Weil A (2011) A new Puercan (early Paleocene) hyopsodontid "condylarth" from New Mexico. Acta Palaeontol Pol 56:247–255.

Wilson GP (2014) Mammalian extinction, survival, and recovery dynamics across the Cretaceous-Paleogene boundary in northeastern Montana, USA. In: Wilson GP, Clemens WA, Horner JR, Hartman JH (eds) Through the End of the Cretaceous in the Type Locality of the Hell Creek Formation in Montana and Adjacent Areas. Geol Soc Am Spec Pap 503, Boulder, pp 365–392.

Wilson Mantilla GP, Chester SGB, Clemens WA, Moore JR, Sprain C, Hovatter BT, Mitchell WS, Mans WW, Mundil R, Renne PR (2021) Earliest Palaeocene purgatoriids and the initial radiation of stem primates. R Soc Open Sci 8:210050.

Zack SP (2009) The phylogeny of eutherian mammals: a new analysis emphasizing dental and postcranial morphology of Paleogene taxa. Dissertation, Johns Hopkins University.

Zack SP, Penkrot TA, Bloch JI, Rose KD (2005) Affinities of 'hyopsodontids' to elephant shrews and a Holarctic origin of Afrotheria. Nature 434:497–501.

Ziegler AC (1971) A theory of the evolution of therian dental formulas and replacement patterns. Q Rev Biol 46:226–249.